A Microfluidic Device for Transfection of Mammalian Cells Using Adjustable Shear Stress

Veronika Cencen

A thesis submitted to the
Faculty of Graduate and Postdoctoral Studies
in partial fulfillment of the requirements for the
Master of Applied Science in Biomedical Engineering

Department of Biomedical Engineering
Faculty of Engineering
University of Ottawa

Abstract

Microfluidic technology is a rapidly progressing tool in biomedical engineering. Microfluidic devices are appreciated for their simplicity and production efficiency potential. Our research focuses on developing a microfluidic device capable of transfecting cells by applying shear stress to cause temporary membrane damage. The advantage of this physical method of transfection is the possibility of incorporating large molecules that cannot be inserted with more traditional chemical transfection methods, while avoiding the large fall in viability seen with other physical methods such as electroporation. Unlike previous groups, our device incorporates the use of microfluidic valves to allow tunability, and impedance sensing for cell membrane damage analysis. We achieve (95±5)% cell viability and up to (68±5)% efficiency in transfecting 3T3 cells with DNA-sized molecules. In future stages, we intend to add the device onto an existing cell-encapsulation device that is tasked with preparing therapeutic cells to be used in regenerative medicine applications.

Statement of Originality

The content presented in this document is, to the best of the author's knowledge, the product of original work performed by the author at the University of Ottawa under the supervision of Professor Michel Godin.

In partial fulfillment of the requirements for the degree of Master of Applied Science (Biomedical Engineering) at the University of Ottawa, this work was presented at the Ottawa Carleton Institute for Biomedical Engineering Seminar Series:

Cencen V. and Godin M. Transfection Of Mammalian Cells Using Shear Stress In Microfluidic Devices. Ottawa Carleton Institute for Biomedical Engineering. November 2015.

Statement of Contributions

The author wrote the main body of this work, with credited contribution of standard laboratory protocols in the Appendix. The author also contributed to the photomask design, the microfabrication, and the testing of devices, with contributions from Dr. Benjamin Watts. The LabVIEW® code was created by Prof. Michel Godin and adapted by the author and by Eric Beamish. The experimental setup was assembled by the author and by Prof. Michel Godin. All cultured cells and cell culture resources were obtained from members of the Pelling research group at the University of Ottawa and maintained by the author. Unless referenced in the caption with obtained permissions, the author created all figures in this thesis.

Acknowledgements

I wish to express my gratitude to my supervisor Prof. Michel Godin, who facilitated my transition from a biotechnology undergraduate to an experimental researcher and engineer in nanotechnology and biophysics with great efficiency. I would like to add my appreciation for his support and guidance in balancing my academic and athletic careers.

I am also grateful to Dr. Benjamin Watts for introducing me to the process of microfabrication and experimental work in microfluidics, Dr. Tina Haase for helping me expand my practical skills in cell culturing and image analysis techniques, and Lukasz Andrzejewski for his assistance in using LabView. Additional thanks is given to the members of the Pelling Lab group for their assistance in accessing cell culturing and imaging resources. I was also fortunate to have a very friendly, supportive and helpful lab group, including Wenyang Jing, Ainara Benavente, Eric Beamish, Radin Tahvildari, Ali Najafi Sohi and Adefemi Adeyemi, as well as Cedric Eveleigh, Keith Dennis Ludlow, Maël Chow-Cloutier and Louise Munro.

There are many others I would like to thank for their support and encouragement, including my coaches, the Let's Talk Science volunteer group, prof. Andrej Kosmrlj at Princeton University, professors from my program, my former professors from the University of Ljubljana, and other friends and relatives. However, I believe a major mention should be given to my parents, Marjan and Lilijana, my junior sister Eva, for standing by me through this major chapter of life and supporting my decisions to any extent possible.

Table of Contents

Legend

ASM	Lysosomal acid sphingomyelinase
AC	Alternating current
BSA	Bovine serum albumin
DMEM	Dulbecco's Modified Eagle's Medium
FBS	Foetal bovine serum
MFI	Mean fluorescence intensity
PBS	Phosphate buffered saline
PDMS	Polydimethylsiloxane
PI	Propidium iodide
PS	Penicillin-streptomycin

List of Figures

List of Tables

List of Equations

1 Introduction and Literature Review

1.1 Background and Significance

Modifying human stem cells for therapeutic purposes has become an increasingly popular and valuable area of interest in the past few decades (Peister, et al., 2004). This includes applications in tissue and organ regeneration. Such work often involves challenging cell types, including stem cells and immune cells, some of which are incapable of endocytosis. Furthermore, cells for use in medical applications are often damaged by forces that they are unaccustomed to. This can become an issue when such forces are involved in critically required research procedures, such as the high level of electric force required for electroporation.

There is great interest for the development of treatments involving stem cells, which unfortunately happen to be both sensitive and challenging to manipulate. Since the main purpose of stem cell therapy is tissue regeneration, it is desirable that cells would regrow the desired tissue quickly and efficiently. Transfecting such cells to express cell proliferation promoting enzymes, such as endothelial nitric oxide synthase (eNOS), is therefore of particular interest (Sueblinvong and Weiss, 2010).

A condition that would benefit from the targeted personalization offered by stem cell therapies is pulmonary arterial hypertension, a progressive disease in which the loss of functional lung microvasculature (narrowing of arteries) causes high blood pressure, and can ultimately damage the right ventricle of the heart (Kwapiszewska et al., 2016). Significant progress

towards a cure has been made using endothelial progenitor cells transiently transfected with endothelial nitric oxide synthase (Granton et al., 2015). With the initial success, it is now possible to seek improvements in terms of throughput, efficiency and accessibility. This may be possible with the increasingly popular technique of microfluidics.

1.2 Introduction to Microfluidics

Microfluidic technology, or the science and engineering of fluids in micro or nano-scale structures, is an increasingly popular tool in science and engineering, with a good outlook towards commercialization in the near future (Volpatti and Yetisen, 2014). Microfluidic devices are becoming increasingly common in university laboratories, where the concepts of a lab-on-a-chip (Dittrich and Manz, 2006) and micro total analysis systems, μTAS (Kovarik et al., 2013) have facilitated research and solved many issues related to availability of materials and space. Also desirable are the shortened transportation time of mass and heat, low energy consumption, and opportunity for parallelization and integration (Dittrich and Manz, 2006). Further functionality can be added to create microsystem technology (MST) and micro-electromechanical systems (MEMS), where electronic and mechanical components are used for further manipulation and analysis of biological samples (Djakov et al., 2014).

One of the most useful traits of microfluidics is the effect of the micro-scale on the Reynold's number, (or comparison of effect of momentum of a fluid to the effect of viscosity of that fluid). This is an important component of the Navier-Stokes equation, Equation 1

$$\rho\left(\frac{\partial u}{\partial t} + u \cdot \nabla u\right) = -\nabla p + \mu \nabla^2 u + f \qquad 1$$

Here, u is the velocity vector field of the fluid, p is the pressure, ρ is the fluid density, μ is the kinematic viscosity of the fluid, and f is the acceleration vector field caused by external forces.

The second term on the left part of the equation is caused by long-term above-micro-scale events such as turbulence. At a micro-scale, these effects are negligible in comparison to the second term on the right, where viscous forces overcome inertial forces. The ratio of viscous and inertial forces required for inertial forces to become negligible can be found through the Reynold's number, where flow length is represented by l, as in Equation 2:

$$Re = \frac{\rho u l}{\mu} \qquad 2$$

When $Re \ll 1$, laminar flow conditions are satisfied (no mixing in the traditional sense), and the Navier-Stokes equation can be simplified to the Stokes equation, Equation 3, which is easier to solve and work with:

$$\rho\left(\frac{\partial u}{\partial t}\right) = -\nabla p + \mu\nabla^2 u + f \qquad 3$$

Among other phenomena, these conditions give rise to Poiseuille's flow; this refers to the fact that the only force affecting the liquid in the channel is from the pressure drop along the length of the microfluidic channel (Laurell and Lenshof, 2015).

In addition, the Segré and Silberberg phenomenon of inertial focusing is also useful, and includes appropriate contribution from the essential forces (wall interaction force, shear gradient lift force, and secondary-flow drag force), channel geometry (length and cross-section), and other parameters (rotation, fluid properties, and particle properties and spacing) (Martel, 2015). The phenomenon refers to how buoyant particles in laminar flow remain at 0.6-radius height of the channel (Segré and Silberberg, 1961); this is quite desirable to prevent sticking of cells to the channel sides, as well as prevention of unwanted shear stress on the cells as they flow through the channel at higher speeds. It should be noted that the phenomenon is likely to become diminished at high (1/3 total sample volume) particle concentrations (Martel, 2015).

Combined, these properties allow better control over physical properties, such as pH, temperature, shear stress, concentration, and other highly desirable properties in single and multi-step reactions, since very small amounts of sample are handled in short amounts of time (Chokkalingam et al., 2010).

1.3 Microfabrication

Microfluidic devices can be fabricated using several methods (Iliescu et al., 2012) (Lake et al., 2015), the most common being soft lithography (Unger et al., 2000). Microfluidic devices must satisfy several requirements: optical compatibility, durability, biocompatibility and other details. Therefore, optimization is crucial at several levels of fabrication. Parameters with highest priority are selected based on application, in this case referring to cell transfection and impedance sensing.

1.4 Microfluidics for Mammalian Cell Transfection

Transfection originally referred to deliberate introduction of genetic material or protein into all cell types. However, with the existence of new terminology for other cell types and methods, this term is most often used for non-viral methods of introducing foreign material into mammalian cells (Promega, 2016). These were introduced by Vaheri and Pagano in 1965 using DEAE Dextran (Vaheri and Pagano, 1965), followed by Graham and van der Eb in 1973, where chemical transfection was performed with calcium phosphate (Graham and van der Eb, 1973). Transfection can be chemical or physical, with further division into subcategories. Some of the most accepted methods along with their main drawbacks are summarized in Table 1.

Table 1: A list of major categories for mammalian cell transfection and their primary deficiencies

Method of Transfection	**Limitations Associated with Method of Transfection**
Transduction (transfection using a viral vector) (Otto-Wilhelm Merten, 2011)	Immunogenicity and cytotoxicity are both major issues for which solutions are continuously being developed. An additional issue would be that using this method, it is not possible to insert large or irregular molecules, such as large proteins.
Chemical methods of transfection, such as lipofection (*Lipofection,* 2008) (Varkouhi et al., 2011)	Certain cell types, such as stem cells, cannot be transfected with these methods. Limited efficiency and endosomal traps pose additional problems.
Microinjection, biophotonics and other single cell methods of transfection (Carroll, 2009)	These methods are limited by their low throughput, since only one cell at a time can be processed.
Electroporation, sonoporation, biolistics, magnetofection, other physical methods of transfection (Das, et al., 2015) (Vandergriff et al., 2014) (Sudowe, 2013)	These methods are limited by low viability, and are often used to destroy cells for research purposes. An acceptable viability to efficiency ratio is difficult to reach, which would be problematic if the method were to be used for medical applications.
Impalefection (delivery with nanomaterials, such as carbon nanotubes, nanofibers, nanowires) (Jinturkar, et al., 2011) (Kim, 2008)	These methods of transfection are relatively unexplored and have limited applicability at their current stage.

A transfection method presented as providing a good compromise between viability and efficiency of cells, with an additional benefit of relatively simple and feasible implementation, was developed by Sharei et al. in 2013. In their research, they describe, as shown in Figure 1, a microfluidic device with narrow constrictions through which the cells are forced to squeeze

at appropriately high flow rates, causing the membrane to temporarily porate (develop small, reversible holes) and allow the desired molecules to enter. According to the authors' claims, this is possible without destroying or killing the cell, since it would heal within seconds of molecule uptake (Sharei, Zoldan et al., 2013) due to the nature and consideration of cell membrane dynamics (Andrews et al., 2014) (Kollmannsperger et al., 2016). Time of healing for eukaryotic cells should be sufficient to allow endocytosis and subsequent degradation of lesions, a process triggered by the release of lysosomal acid sphingomyelinase (ASM) (Andrews et al., 2014). In previous studies, initial experiments were performed on HeLa and 3T3 cells, human foreskin fibroblasts (NuFFs), primary, murine dendritic cells, and embryonic stem cells, as well as white blood cells, T cells, B cells and macrophages. The research by Sharei et al. also showed that both longer constrictions (up to 40μm) and higher flow rates had relatively low efficiency-viability ratios in comparison to using multiple shorter (20μm) constrictions, once again a useful development towards the possibility of use for medical applications (Sharei, Zoldan et al., 2013).

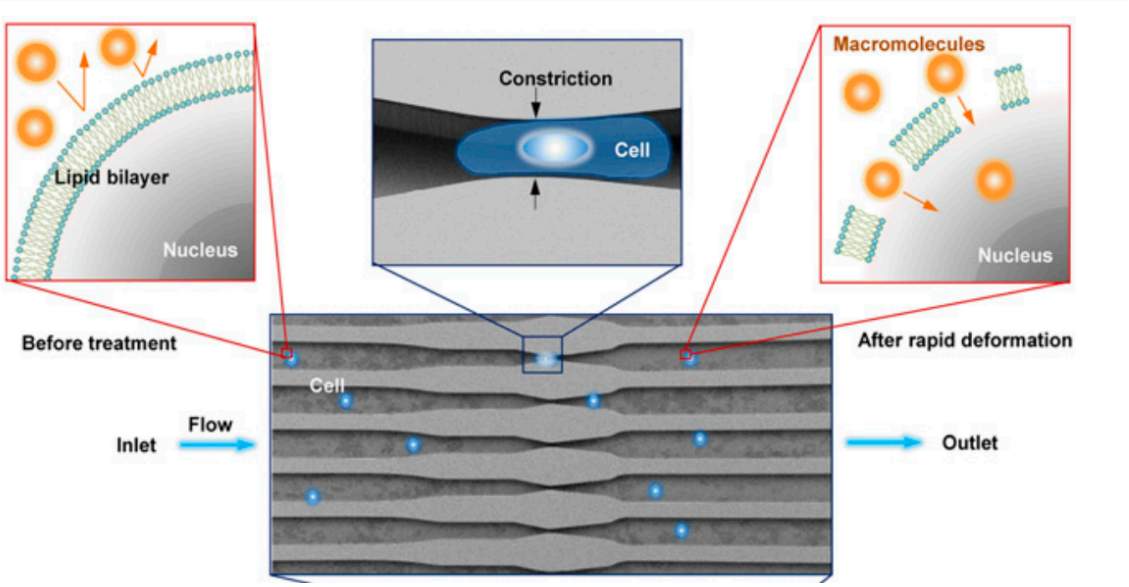

Figure 1: Figure obtained from (Sharei et al., 2013) with permission. A depiction of the channels in the device used by Sharei et al., also showing schematic representation of where the cell is constricted, and how the resulting membrane damage allows nanoparticles to enter through the pores. Blue dots represent the cells flowing, left to right, through the microfluidic channels.

This method of shear stress transfection has since been used in numerous applications involving transfecting sensitive and difficult to transfect cell types (Sharei et al., 2015) and expanding the range and size of material to transfer (Marx, 2016). Several steps have been taken to improve the method, including improved pressure regulation, ergonomics, and range of applications. However, with current devices, the dimensions/extent of constriction have to be adapted for each cell type and transfection material. To solve this limitation, we introduce flexible valves used to actively control the constriction height without stopping the flow. In this way, the same device may be used for a range of cell and transfection material shapes and sizes, potentially inputted from various preliminary channels.

1.4.1 Cell Imaging

Fluorescent imaging is a valuable tool in experimental work involving cells. One example of the use of fluorescence is to test for cell viability. A common and relatively simple way to test the viability of cells is using propidium iodide (PI) staining. Here, a cell with a damaged membrane will allow PI to pass causing the cell to fluoresce red (Gou et al., 2011). Furthermore, Sharei et al., 2013, used fluorescent labels such as Fluorescein to track the particles they wished to insert into cells (Sharei et al., 2013). It is therefore important to understand the fundamentals of the standard procedures of fluorescent imaging, and be aware of its potential drawbacks. A relevant consideration for this project was the phenomenon of photobleaching, the loss of fluorescent signal overtime (Fluorescence Fundamentals, 2015).

The fluorescent dye Fluorescein is subject to photobleaching, particularly during prolonged exposure to fluorescent light for the purpose of obtaining images (Hinkeldey, Schmitt, and Jung, 2008) (Spence, Johnson 2010), and likely in some extent during prolonged exposure to white light during experimental runs (Song, Hennink, Young, and Tanke, 1995). An example for the effects of photobleaching from work done by other researchers is shown in Figure 2. While photostability enhancers are available and found to significantly decrease this effect, they are highly likely to damage the cell viability (Widengren, Chmyrov, Eggeling, Löfdahl, and Seidel, 2007), and were not used in the work presented in this thesis. Fluorescence can be used as a qualitative rather than quantitative experimental result by observing the presence or absence of expected signal.

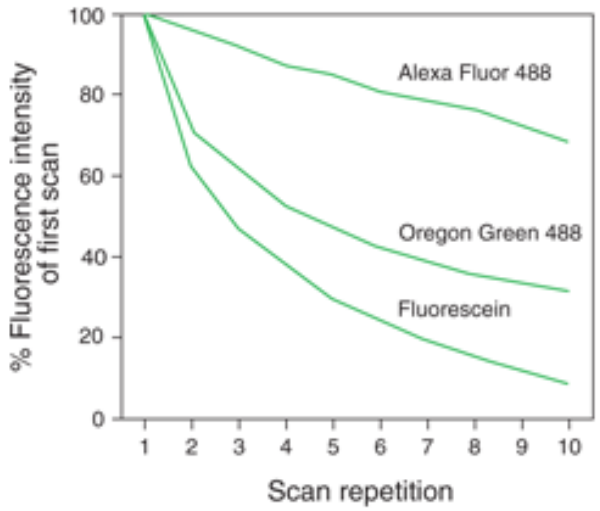

Figure 2: Taken from (Fluorescence Fundamentals 2015). Photobleaching effect for various fluorescent dyes, including fluorescein (used in our work), in this case during laser-scanning cytometry. The authors describe:

"Photobleaching resistance of the green fluorescent Alexa Fluor 488, Oregon Green 488 and Fluorescein dyes, as determined by laser-scanning cytometry. EL4 cells were labelled with biotin-conjugated anti-CD44 antibody and detected by Alexa Fluor 488 (S11223, S32354), Oregon Green 488 (S6368) or Fluorescein (S869) streptavidin (Avidin, Streptavidin, NeutrAvidin and CaptAvidin Biotin-Binding Proteins and Affinity Matrices—Section 7.6). The cells were then fixed in 1% formaldehyde, washed and wet-mounted. After mounting, cells were scanned ten times on a laser-scanning cytometer; laser power levels were 25 mW for the 488 nm spectral line of the argon-ion laser. Scan durations were approximately 5 minutes, and each repetition was started immediately after completion of the previous scan. Data are expressed as percentages derived from the mean fluorescence intensity (MFI) of each scan divided by the MFI of the first scan. Data contributed by Bill Telford, Experimental Transplantation and Immunology Branch, National Cancer Institute."

1.5 Microfluidics for Impedance Sensing

The use of cell impedance measurement to assess cell membrane damage is seen as a potentially valuable tool for allowing immediate identification of compromised cell membrane integrity. An extension of the work towards a new method of cell transfection presented here was to integrate a method of testing the cell membrane integrity on-chip. Being able to sense when the cell becomes damaged to a sufficient extent, while the cell transfection experiment is being run, was one of the challenges recognized by previous researchers working on mammalian cell transfection using shear stress (Sharei et al., 2014). A solution to this challenge proposed by previous work on cell transfection using other methods, particularly electroporation, was to use immediate post-transfection microfluidic single cell impedance sensing. This technique was also used in analyzing single cell recovery from the irreversible electroporation (Bürgel et al., 2015). Prior to exploring the details of the possibilities, it is necessary to familiarize oneself with the background of single cell impedance measurement and the possible research methods involved.

The electrical properties of single cells are a well-explored field with a wide range of applications (Gou et al., 2011) (Chen et al., 2015) (Mansor and Ahmad, 2015). Current knowledge and understanding of the topic is valued at various stages of research. Currently, one of the most common applications of impedance sensing involving mammalian cells is cell size sorting (Clausen et al., 2014), as well as basic cell counting, or impedance cytometry (Sun and Morgan, 2010). The basis for electrical behaviour of single cells in suspension is the single cell electrical model. Transmembrane potential, ΔV_m, induced in a cell by an applied field, E, is given by the Equation 4:

$$\Delta V_m = \delta E r \cos\phi \quad (4)$$

In this equation, δ is the weighting factor that quantifies the impact of the cell on the extracellular field distribution, r is the radius and ϕ is the polar angle with respect to external field (Wang and Lu, 2006). An electrical model of a single biological cell is shown in Figure 3.

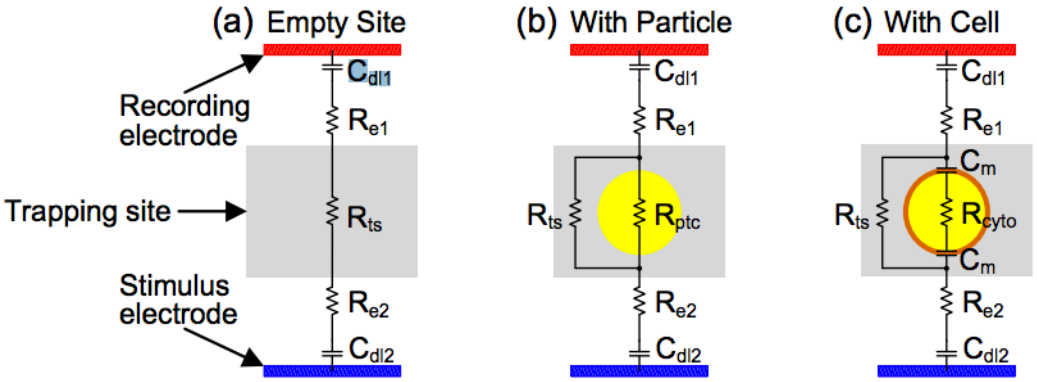

Figure 3: From (Zhu et al., 2012) . Equivalence circuit model schematic representations for (a) an empty space between two electrodes, (b) a particle between two electrodes (c) a biological cell between two electrodes.

C_{dl1} and C_{dl2} are double layer capacitance for each electrode, R_{e1} and R_{e2} is resistance of bulk medium around the recording and stimulus electrode respectively, and R_{ts} is resistance of the bulk medium across the trapping site. A particle will add a resistance R_{tps} parallel to the R_{ts}. By comparison, a cell membrane will add a capacitive component C_m (detectable at higher frequencies), and a resistance of the cytoplasm, R_{cyto}.

The resistive components are the 'real' parts of the equation and have an impedance independent of frequency of AC current applied. The capacitive, 'imaginary' components' impedance decreases with the increased frequency, and is phase shifted 90° with respect to voltage. The contribution of each of these two components, the real and imaginary, can

therefore be observed in both magnitude and phase shift of the signal. In other terms, the impedance is composed of signal magnitude and signal phase shift. For the purpose of work presented in this thesis, measurement of signal magnitude was considered sufficient. Notably, the main component that adds complexity to impedance measurement of cells as opposed to particles is the presence of the membrane, which, unlike the cytoplasm and particles, behaves as a capacitive component, and therefore adds a frequency-dependent imaginary part to the equation. The resistive and capacitive components are added in parallel to the electrode and inter-electrode area contributions, giving the impedance Equation 5 below:

$$Z_{cell} = R_{e1} + R_{e1} + \frac{1}{j\omega C_{dl1}} + \frac{1}{j\omega C_{dl2}} + R_{ts} \parallel (R_{cyto} + \frac{1}{j\omega C_m}) \qquad 5$$

Particle and cell resistance was found to contribute to the impedance at frequencies below 1MHz, while cytoplasm resistance becomes dominant at frequencies above 10MHz, where the membrane is polarized and cytoplasm currents are induced (Gawad et al., 2004).

To measure these components in microfluidic devices for impedance sensing, the primary requirement is a sensing volume with an electric current flowing through it, which is usually achieved by applying a voltage to a pair of electrodes by which the cell passes. A passing cell causes an increase in impedance due to the displacement of ions. The amplitude of the resulting current drop depends on several parameters related to the cell, its surroundings, and the measuring equipment (Zheng et al., 2013). Significant progress has been made since the origins of impedance sensing, which started with the simple counting and sizing of cells with

a Coulter Counter (Fritzsch et al., 2012). This included advances in microelectrode design, as well as the introduction of alternating current (AC) input potential (Riordon et al., 2014). Among other benefits in signal acquisition quality and refined operation, these enabled researchers to observe and monitor several other cellular components in addition to its size, particularly when reaching higher frequencies.

Improvements are continuously being made towards efficient, sensitive measurement of various components of cells. While low frequencies will sense mainly the size-dependent resistance, higher frequencies can detect the conductive intracellular cytoplasm. This is useful in analyzing subcellular components, but also for detecting changes in cell membrane integrity to higher precision. When a cell's membrane is damaged or porated, the impedance-related current (or voltage) signal reversal (corresponding to a switch to sensing of the cytoplasm rather than the cell membrane) is not visible to the same extent as with healthy cells (Cheung et al., 2010), and with sufficient damage might not reverse at all (Bürgel et al., 2015) (Gawad et al., 2004) (Mansor and Ahmad, 2015). At lower frequencies, the cell membrane capacitance shields the interior of the cell from the electric field, causing a drop in current (or corresponding calculated voltage) when the cell passes the electrodes, and this remains the case for both the intact and porated cells. At higher frequency levels, the electric field can pass the membrane and detect the conductive cytoplasm, hence reversing the signal. If the cell is damaged the conductive effect of the cytoplasm is diminished as it merges with the surroundings through the pores (Bürgel et al., 2015). A summary of such findings by other researchers is shown in Figure 4 below. Frequencies in or near the MHz range are therefore required to clearly distinguish damaged and intact cell membrane, while avoiding parasitic capacitance (Bürgel et al., 2015) (Pierzchalski et al., 2010).

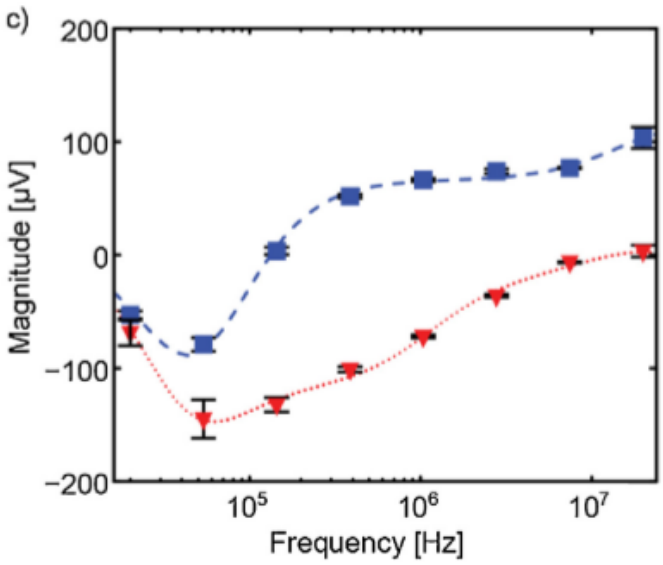

Figure 4: Taken from (Bürgel et al., 2015) with permission. The voltage magnitude component of the impedance signal for a single HeLa cell before (blue) and after (red) cell membrane damage (With electroporation). A summary of the original authors' description: Magnitude of one single HeLa cell before and after electroporation: measured values are represented as squares (before electroporation) and triangles (after electroporation); the model fits are represented by blue dashed and red dotted lines. The spectra are presented after baseline subtraction. All EIS results are from the same HeLa. Error bars indicate the standard deviation for five measurements of the same single cell by shuttling the cell back and forth.

Applying AC to a cell at high enough voltages is also used in electroporation, a membrane damage technique often used for cell transfection. This method can be used to extract material and information from within the cells. When transmembrane potential surpasses a threshold (found between 0.1-1.1V), the cell reaches reversible electroporation, forming membrane pores (or openings) tens of nanometers in diameter (Chang and Reese, 1990) (Teissié and Rols, 1993). In impedance sensing, we wish to avoid this membrane-damaging effect during

the measurements. Voltage of the stimulation electrode must therefore be kept sufficiently low, but allow sensing of the cell under normal and damaged membrane conditions (Gou et al., 2011). Considering distance from electrodes and interference of suspension solutions, voltages of 1V or below can be considered appropriate for measurements in microfluidic devices (Bürgel et al., 2015). Distance between the stimulation and recording electrodes is also a key factor to consider (Gawad et al., 2004) and is usually set at approximately the cell diameter to allow optimal compromise between field uniformity, detection range, and detection sensitivity (Clausen et al., 2014) (Sun and Morgan, 2010).

Exposure to shear stress is expected to change the impedance of cells due to changes in the plasma membrane integrity in a similar way (Kurz et al., 2010). However, the settings must be carefully calibrated for the application (Chen et al., 2015), since impedance sensing will sense different cell properties depending on the frequency domain, as shown in Figure 5 below (Gawad et al., 2004) (Coster et al., 1996).

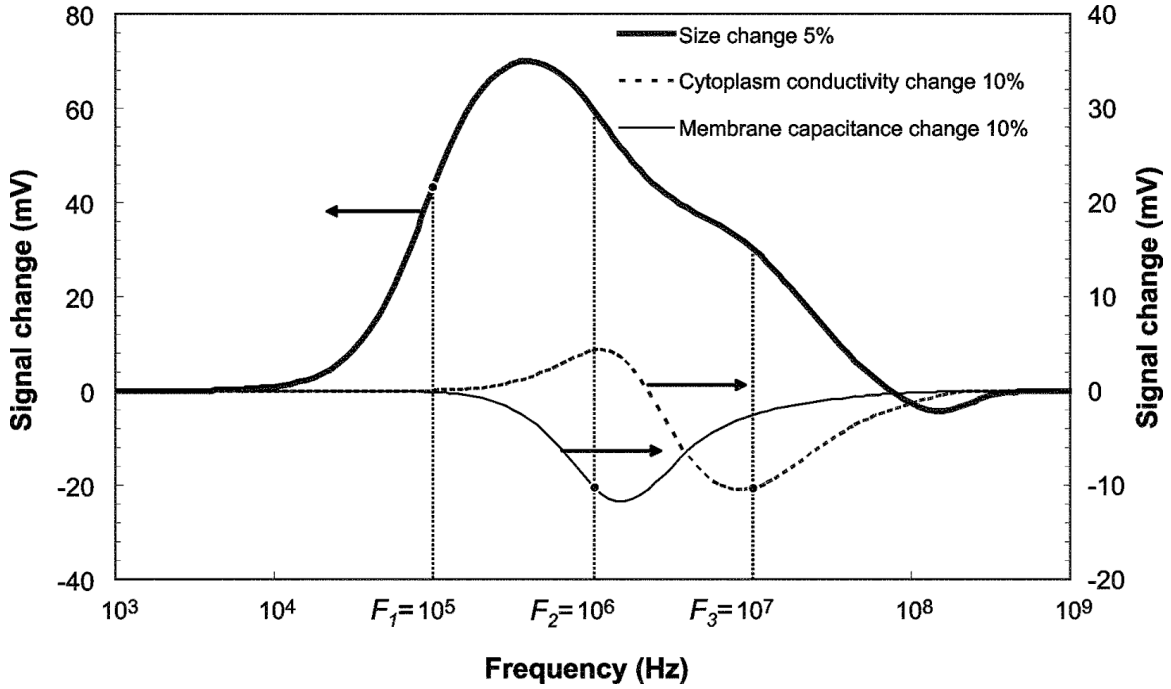

Figure 5: Taken from (Gawad et al., 2004) with permission. Simulated signal amplitude changes in Voltage signal at the amplification output with variation in the modelled cell properties (phase information is neglected). From this model it is possible to see how small changes in cell size affect the full spectrum. At 100kHz changes due to other parameters are relatively small. Change in other cell parameters influence the spectrum in different ways at higher frequencies.

Unfortunately, using cell impedance sensing for such a complex application is a challenging and not yet fully developed method. Nonetheless, it is a popular choice for research in cell biology, and with appropriate attention and development, it may prove increasingly useful in applications of higher complexity. While input frequency and voltage amplitude are recognized as major control parameters in terms of cell damage and measurement efficiency, it is understood that transit time (calculated from flow speed), channel geometry, electrode geometry, suspension medium of cells, and other parameters and noise sources must also be considered. These were some of the challenges we considered, and overcame as much as possible, in the work presented in this thesis.

1.6 Objectives

The purpose of this study was to modify and add on to an existing method of shear stress based transfection, which could eventually lead to more universal applicability and enhanced performance of the device. In addition, we aim to add on-chip damage assessment of cell membrane through impedance sensing, where signal magnitude changes, or even complete signal reversal, may differentiate reversible poration from healthy cells and irreversibly destroyed cells. The study was divided into work on two devices – one for tunable transfection, and one for impedance sensing – which were then combined into one device.

2 Methods

The broad goal of this work is to design a microfluidic device capable of performing mechanical transfection on mammalian cells using a channel constriction with tunable dimensions. This tunability will allow the accommodation of cells having different dimensions. An on-chip cell impedance sensor will also be included to assess the efficiency of the mechanical transfection imposed on the cells, by way of measurement of the cell membrane capacitance. Cell membrane capacitance is related to its porosity, which will increase as the cell is exposed to increased shear stresses. Transfection and impedance sensing capabilities were assessed independently before being combined into a single device.

2.1 Transfection

2.1.1 Designs

Devices were designed to enable compression of cells as they flowed through constricted microfluidic channels. On-chip valves were used to control the cross-sectional area of the

microfluidic channels, allowing for control over the degree of constriction. Two on-chip channel and valve architecture designs were considered. The first design uses a push-up valve, where cells flowing through a microfluidic channel are constricted by adding pressure to a valve channel below. The cells are pushed upwards towards the top surface of the microfluidic channel wall to the desired extent. The second design has a wall-shaped polydimethylsiloxane (PDMS) barrier in the channel, which the cells have to squeeze past when pressure is applied to the valve channel. Details and corresponding figures are provided later in this section.

Devices were first designed using the CAD program software CleWin4, which is used for printing a photomask (CAD/Art Services) of 10μm resolution for use in photolithographic fabrication as described in Appendix I. Each design was made in a minimum of three repetitions per photomask for the purpose of fabrication efficiency, and in case of imperfections. Alternative minor variations in dimensions were included for potential further testing.

The first designs are referred to as push-up valve designs. These devices achieved cross-sectional tunability by placing a thin membrane with a microfluidic channel below the main flow channel; pressurizing this channel would cause the membrane to displace upwards and compress the channel above (Unger et al., 2000). A model of the first design (push-up valve) in basic form is shown in Figure 6 below.

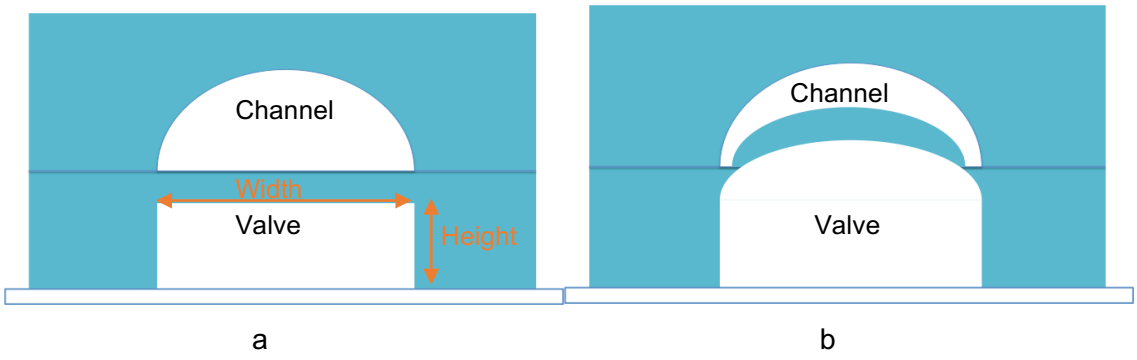

Figure 6: A simplified visual representation of the cross section of a microfluidic device with a push-up microfluidic valve in a) relaxed state and b) the valve pressurized.

Five channel width (50µm, 100µm, 150µm, 200µm, 400µm) and five valve width (10µm, 20µm, 40µm, 50µm, 100µm) dimension combinations were designed and tested. Channel height was constant at 40µm to allow a range of cell sizes to pass comfortably before and after constriction, while keeping the cross sectional area sufficiently low to allow control over flow of cells in the channel. Preliminary testing showed a minimum 1:10 height to width ratio is required to prevent the channel from collapsing upon fabrication. Multiple constrictions for chosen dimensions were included by designing the channel as a serpentine shape.

The main issue for this design was found to be the uneven compression of the main channel across its width, as will be discussed further in the later sections. Additionally, the requirement for a very thin valve membrane for even compression made the devices prone to damage, and made it more challenging to sufficiently damage the cell membrane for mechanical transfection.

The presence of the aforementioned issues prompted the design of the second, barrier-valve

devices, shown in Figure 7. As the name suggests, a barrier is included in the channel of the device by which the cells have to squeeze if there is pressure in the valve channel below. Since the barriers were not attached to the valve, a negative pressure on the valve or a positive pressure on the channel will result in the valve moving away from the barrier, allowing particles and cells to pass. These device designs needed to possess the qualities required for even compression, reliable transient membrane damage, and improved fabrication efficiency. It was possible to increase the width of the valve to 200μm since this did not define the distance of constriction; distance of constriction was instead defined by the width of the barrier. This created a wider valve curve radius and minimized the effects of uneven compression, particularly at increasing constrictions. In addition, the pointed edges of the barrier created conditions for greater shear stress due to reduced surface area. Consequentially, the cell was more likely to be damaged by the softer elastomeric device material. In terms of durability, less stress is placed on the thinner bottom layer of the device, allowing it to last longer.

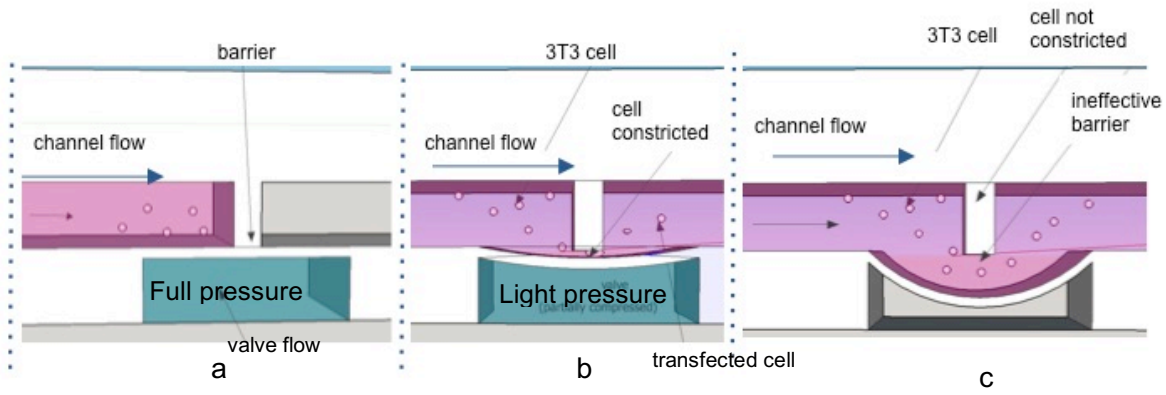

Figure 7: A 3D model of the barrier-valve device when a) channel and valve are fully pressurized, b) valve is partially pressurized and retracts from the barrier, allowing cells to squeeze through, and c) channel is pressurized but valve is not, which retracts it from the barrier entirely, allowing cells to pass freely.

By adding multiple constrictions to this design, as shown in Figure 8, it was possible to approximately replicate the increased efficiency found in previous research (Sharei et al., 2013), while maintaining a high level of viability. Based on previous literature and by confirming with tests, it was assumed that setting the number of constrictions at five was the limit to which the efficiency of transfection would still be increased. The compact design of the devices was retained using a serpentine shape rather than a linear one when adding constriction barriers. By adding pressure to both ends of the multiple constriction device, as described in the next section, it was possible to maintain equal distribution of compression across all five barriers.

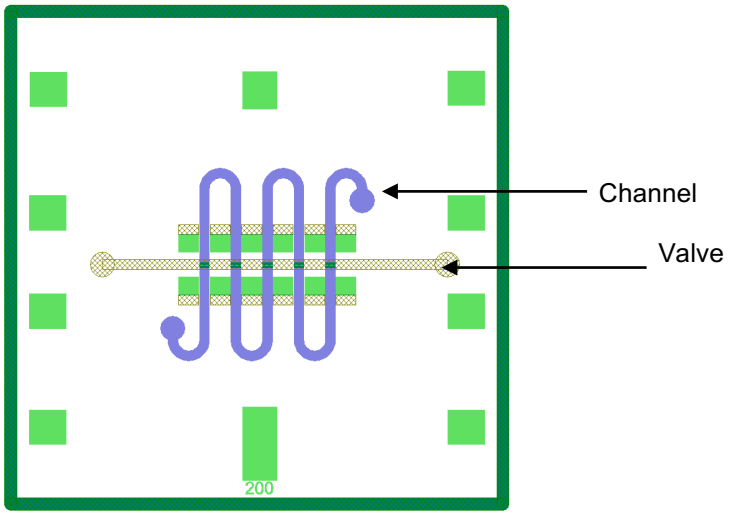

Figure 8: A CleWin4 design for multiple constriction version of barrier-valve transfection devices. Stamp, valve and channel layer are overlapping. The 200µm wide channel is shown in purple, the valve layer in yellow, and the stamp in green. A constriction occurs on each intersection of the channel and valve.

2.1.2 Experimental Setup

The fluidic samples were contained in small vials connected to a pressure source, with tubing

inserted from the vial to the device to allow the fluids to enter the device upon pressurization. Pressure levels were controlled through manual pressure regulators for each vial. Input pressures were kept above output pressures at all times to prevent backflow. A schematic representation of the controlled pressures is shown in Figure 9.

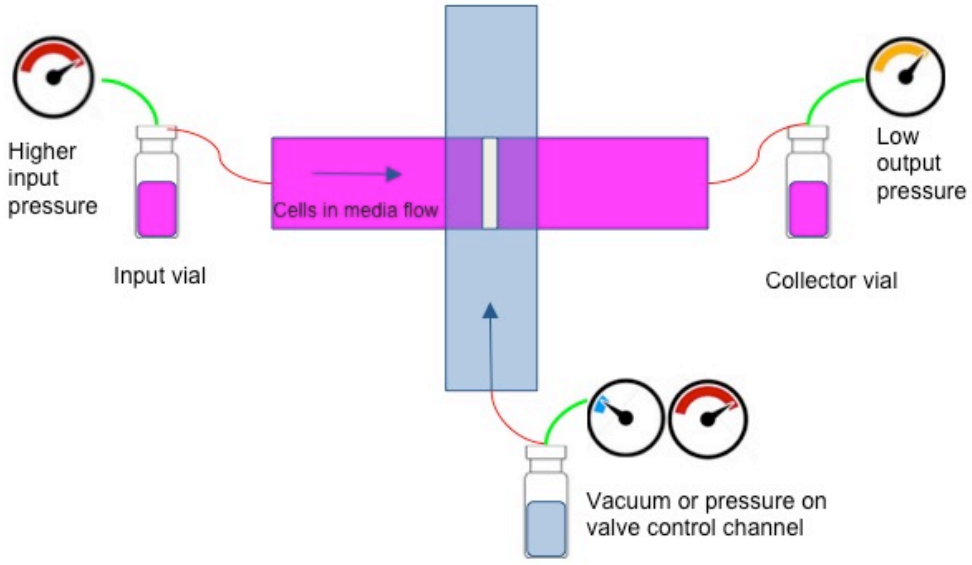

Figure 9: 2D schematic representation of pressure system for barrier-valve transfection device in operation, not to scale. The pink area represents the channel with media and cells, while the blue area represents the valve filled with water. The input pressure must be kept higher than the output to prevent flow in the opposite direction. Pressure levels are generalized due to variation between setups.

2.1.3 Device Fabrication

The microfluidic devices were fabricated using standard multilayer soft lithography (Unger et al., 2000). This allows ease of fabrication, reduction in size, biocompatibility and possibility of easily adding multiple layers, including flexible valves and pumps (Harris et al., 2007).

Moulds for the microfluidic devices were created using a process known as photolithography. After performing a piranha etch and plasma cleaning of a silicon wafer, the appropriate photoresist (SU-8 or AZ) (MicroChem) was deposited using a spin coater (Laurell Spin Coater WS-400BZ-6NPP-LITE) onto a wafer, with spin speed dependent on the desired feature height. Following a soft bake step, the coated wafer was aligned below the photomask and exposed to ultraviolet (UV) light at appropriate exposure time (OAI DUV/NUV mask aligner, model 206). Following a post-exposure bake and development, the feature height was verified using stylus profiler (Veeco/Sloan Dektak 3 30).

The resulting master mold can be reused several times to create PDMS devices as part of the process named multilayered soft lithography with PDMS moulding (Sylgard 184 elastomer kit), a soft non-cytotoxic material ideal for reducing cell death (Alrifaiy, Lindahl, and Ramser, 2012). PDMS was created by mixing the siloxane base and the curing agent provided in a kit. Several layers of PDMS devices can be bonded together and to glass surfaces following plasma treatment. *Details on fabrication processes are provided in Appendix I.*

2.1.3.1 Microfabrication of push-up valve transfection devices

Channel master moulds were created using AZ photolithography to allow for a rounded geometry, while valve master moulds were created using negative SU-8 photolithography, creating relatively robust and angled channel profiles. Both were then moulded with PDMS.

2.1.3.2 Microfabrication of barrier-valve transfection devices

Master molds were created using negative SU-8 photolithography and moulded with PDMS. The design is partially based on the “seat valve” principle of Mosadegh et al. (Mosadegh et

al., 2010), allowing a more evenly distributed compression pattern in comparison with normal push-up valves. This involves a step in fabrication where a specifically designed PDMS stamp is briefly pressed against the barrier sections of the device, deactivating the plasma treatment in that part, and preventing attachment to the valve layer to which the channel layer is aligned and attached. This step is shown in Figure 10.

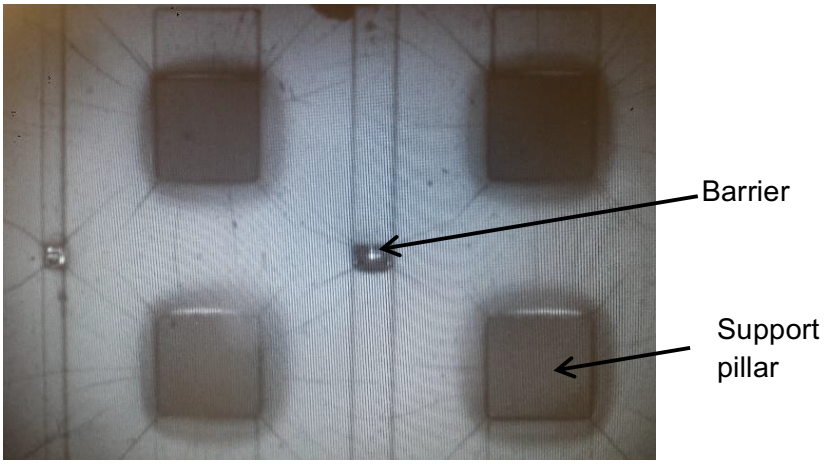

Figure 10: A microscope image showing deactivation "stamping" of embossed PDMS sections of the channel layer that we do not wish to bond to the valve layer. The large squares are used for alignment assistance and stability, to prevent the layers from becoming attached on the sides during deactivation. The small rectangle in the center is the deactivated barrier in the channel.

Following extensive testing of various parameters and designs, the following dimensions, presented in Table 2, were determined appropriate for data collection:

Table 2: Dimensions of channel of microfluidic device determined crucial to its function, adapted from (Sharei et al., 2013)

Parameter	**Dimension (±1μm)**
Channel width	200μm or 400μm
Channel height (valve and channel layers)	50μm
Bridge width	10μm, 20μm, or 40μm

In order to improve transfection efficiency and viability, previous researchers (Sharei et al., 2013) increased the number of constriction repetitions to five, allowing increased efficiency without increasing flow speed, as flow speed increase was shown to cause reduced viability. Due to pressurization on both the input and output of the channel and valve, the compression was even across all five barriers. Figure 11 shows the multiple-constriction device in a relaxed state, and when cells are flowed at 9μm constriction at barriers.

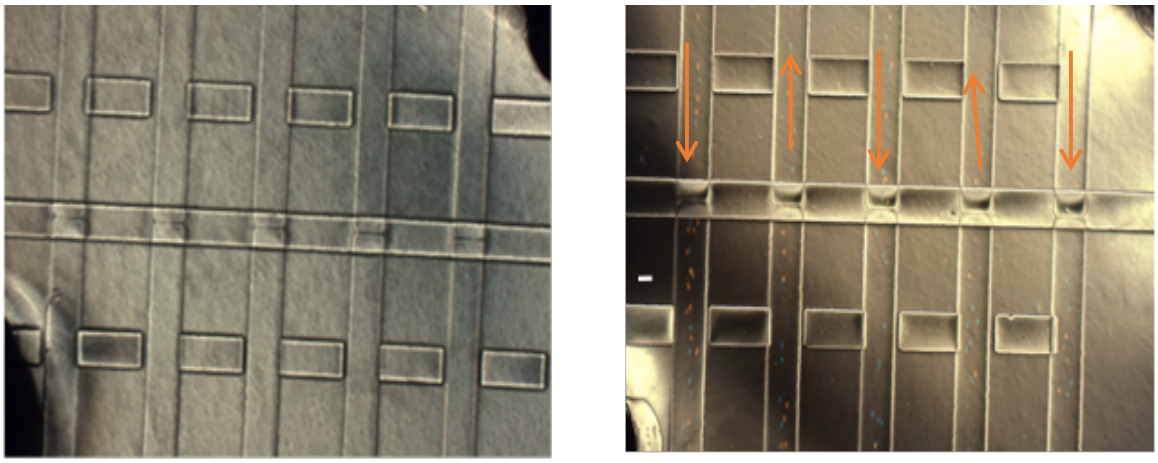

Figure 11: Multiple constriction version of barrier-valve device in relaxed state (left) and operating state (right). In the first image the entire system is not pressurized. The second image the pressures are set for cell transfection (pressurized valve and channel). The scale bar represents 100μm. Orange arrows represent direction of flow for the cells; the valve, seen running horizontally across, is pressurized from both directions.

2.1.4 Calibration

Calibration for push-up valve devices was done by measuring the intensity of fluorescent dye as it was flowed through the device. The intensity of the fluorescence corresponds to the extent of compression as shown in Figure 12.

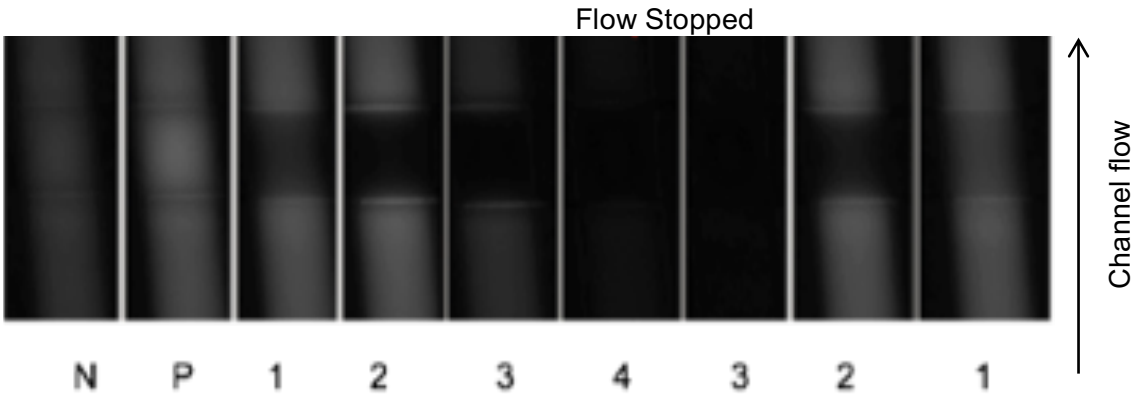

Figure 12: Fluorescent microscopic images of Fluorescein flow through a microfluidic channel. The images show the channel in vertical orientation with a valve channel across it. From the initial unpressurized system (N), the channel is pressurized (P), and the fluorescence gets dimmer in the area of the valve as the valve is closed by adding pressure to the valve channel (labelled as level 1-4). Once the valve is entirely compressed, the flow is stopped, and fluorescence in the channel diminishes.

Intensity was then matched to a known change in channel height and used to identify the approximate depth of compression using a contour plot in Origin, as shown in Figure 13.

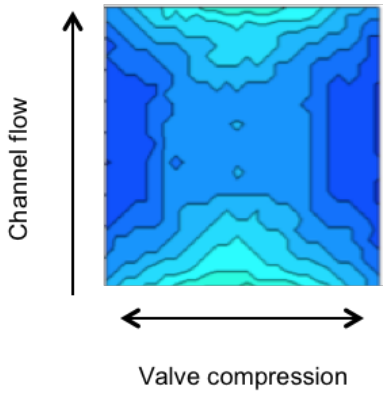

Figure 13: Example of Fluorescein calibration of channel compression (200µm by 200µm). Extent of fluorescence is linearly related to channel height. Uneven compression, particularly in the direction of flow, is evident from this image, particularly at the edges of the valve with the channel. Each step change in shade of blue from dark to light represents a 1µm increase in channel height.

Due to the difference in PDMS thickness at the barrier, a fluorescence flow calibration as done for push-up valve devices was not possible for barrier-valve devices. Instead, constriction height was estimated by stopping beads of various diameters (a process shown in Figure 14), and creating linear regression models allowing estimation of constriction at various device geometries and flow speeds.

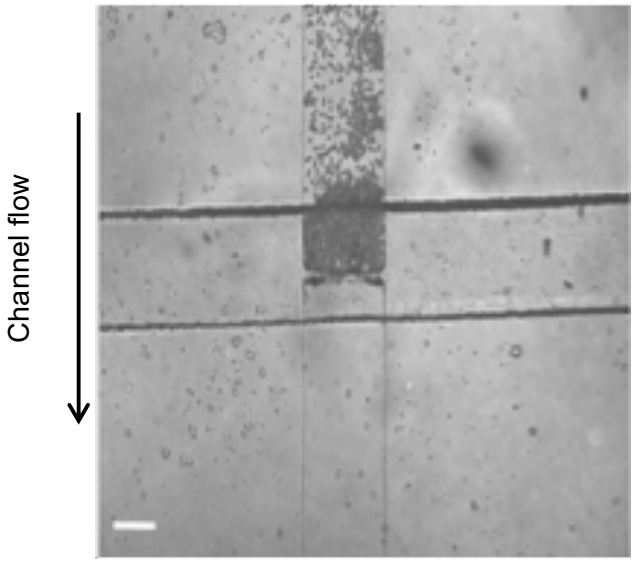

Figure 14: Polystyrene beads, 9μm in diameter being stopped by the barrier of a barrier-valve device when the valve is pressurized. The scale bar represents 100μm. The beads represent the approximate height to which the cells will be compressed in an experimental run.

Various sizes of beads in a span-80 solution were flown through the device and a series of constant channel pressures and valve pressures required to stop the microbeads (without stopping the flow of liquid) were recorded a minimum of five times per condition. Pressure required to compress the 3T3 cells to at least 50% of their diameter in suspension (the diameter of 3T3 cells having been estimated at 18μm) was extrapolated from the linear regression, such as the one shown in Figure 15. Large beads were not used to avoid damage to device and clogging.

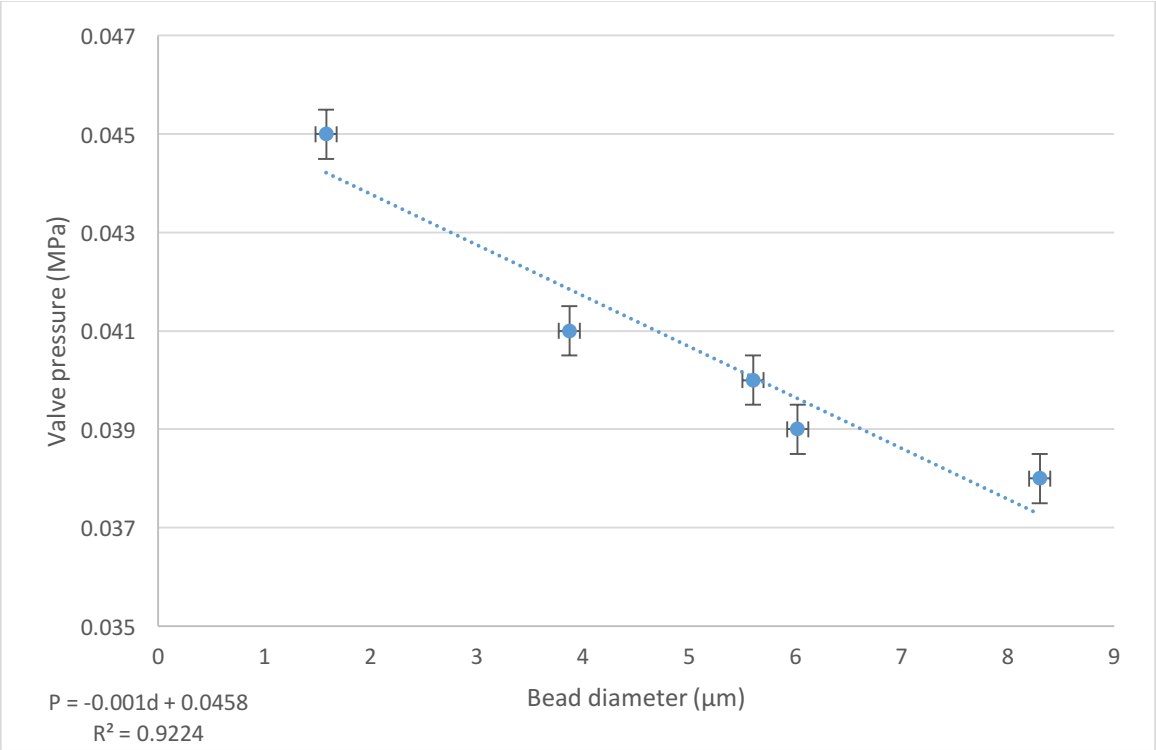

Figure 15: An example calibration model for (0.050±0.005)MPa input pressure and (0.025±0.005)MPa output pressure for the channel, for the most frequently used barrier-valve device geometry, (200µm channel width, 200µm valve width, 20µm barrier width. Channel height is constant.). Error bars present 2SE for three trials per setting. A linear fit was performed (where P represents pressure and d represents diameter), and the resulting equation used to calculate pressures required for other compressions, including the 9µm considered ideal for 3T3 cell transfection. This made it possible to avoid damaging the devices by testing with large sizes of beads

2.1.5 Transfection

The immortalized mouse fibroblast 3T3 cell line was chosen as the model for ease of acquisition and culturing (Todaro and Green, 1963), which is described in Appendix 1. By using robust 3T3 cells, we were able to explore the effects of a wider range of conditions and device designs. Cells were cultured on plates using DMEM supplemented with 1% penicillin-streptomycin (PS) and 9% Fetal bovine serum (FBS) (Hyclone). To prepare suspended cells

for use in microfluidic devices, cells were detached through the standard procedure involving trypsinization. Cells were split after reaching 70-90% confluency to avoid damage, peeling and contamination (Schantz and Ng, 2005). Viability of cells was tested using a PI viability assay; this also allowed distinguishing between necrotic, apoptotic and normal cells (Lecoeur, 2002). A live stain was not performed for transfected cells due to interference of the resulting green fluorescent signal that happens to be of similar wavelength. Furthermore, the live stain was not found to be required, since the main interest was cell death as a result of physical damage, while the cells are suspended (Fink and Cookson, 2005).

To test the ability of the device to transfect cells, the aim was to insert 3-5kDa Fluorescein isothyocyanate (FITC) - labelled dextran molecules, which were chosen to mimic the size of nucleic acids (DNA or RNA), through the cell membrane pores created using the device. To prepare samples, a concentration of cells between 10^6 and 6×10^6 cells was re-suspended in 1% BSA to prevent clogs, 9% 2M KCl to enhance signal, and (0.2±0.1)μg/mL final concentration of 3kDa FITC– labelled dextran. These samples were placed in vials and connected to the pressure setup. Cells (at an approximate concentration of (5.0±0.7) $\times10^6$ cells/mL) were run through a device at the selected pressures. As a negative control, cells from the same passage were left sitting in the same dextran solution without being treated in the device, in order to check for whether similar results would be possible with endocytosis. Another set of cells was left to sit in media with no added dextran, in order to test external effects on viability. After collecting the cells at the output, they were rinsed three times by centrifugation and resuspension, with the purpose of removing background fluorescence. These cells were plated and left to rest for 30 minutes before performing a viability test using PI and determining transfection efficiency by percentage of green fluorescing cells post-treatment.

2.2 Impedance Sensing

2.2.1 Designs and fabrication

For preliminary tests in impedance sensing, a single PDMS channel layer was bonded to a glass slide patterned with metallic electrodes, as shown in Appendix III. There are various electrode configurations useful in impedance sensing in microfluidics (Chen et al., 2015). Coplanar Cr/Au microelectrodes provide an efficient compromise between ease of fabrication (valuable at the testing stage), while still maintaining an adequate extent of reliability, field uniformity and sensitivity otherwise best obtained with parallel facing electrodes (Clausen et al., 2014) (Chen et al., 2015). Coplanar electrodes across a microchannel are shown in Figure 16.

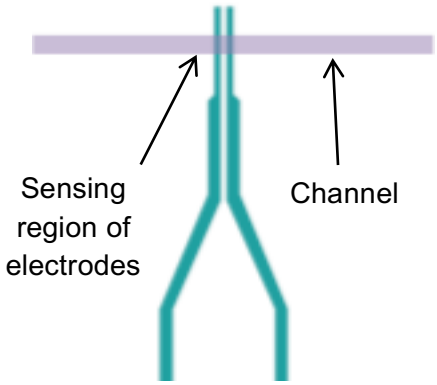

Figure 16: Coplanar electrode design with 20μm inter-electrode spacing, with a close-up of the electrode tips which are important for sensing of cells. The microfluidic channel is shown in purple. The design is an adaptation to 30μm inter-electrode spacing used in a previous laboratory project. Various methods can be used for the Cr/Au deposition on the opaque areas of the design.

The Cr/Au electrodes were fabricated using a wet-etch technique (Hesketh, 1998). This technique provides relatively high fabrication efficiency, but slightly lower electrode sensitivity, found to be sufficient for this application. Chromium is used as the adhesion layer,

while gold is used as the main electrode layer. This method and adaptations made are further described in the Appendix I.

2.2.2 Electronic Setup

Additional images provided in Appendix II

The previously described electrodes were located on the bottom of the device channel. By applying an AC signal to these electrodes, it was possible to measure ionic current between them as a function of frequency.

Figure 17 shows an overview of the electronic setup used for measuring impedance sensing signals. The device received a 0.3V sine wave at a frequency of *N*kHz from a dedicated function generator (Stanford Research Systems DS345) passing through a unity-gain pre-amplifier. The current was then amplified using a current amplifier (Keithley 428). Using a lock-in amplifier (Stanford Research Systems SR830 DSP), the voltage amplitude of the amplified signal could be measured at the drive frequency. The purpose of the lock-in amplifier is to amplify the signal of interest, allowing it to stand out from a background of higher amplitude noise at several frequencies (Wolfson and Mullen, 2010). However, since our lock-in amplifier can only accept signal with frequencies below 100kHz, a frequency multiplier circuit was built and used to down-mix the signal to 50kHz, as discussed below. A second function generator operating at a frequency of *N+50*kHz was used as a reference for the multiplier circuit. A third function generator set to a frequency of 50kHz was used to define the measurement frequency of the lock-in amplifier. The lock-in signal was then recorded using a data acquisition card.

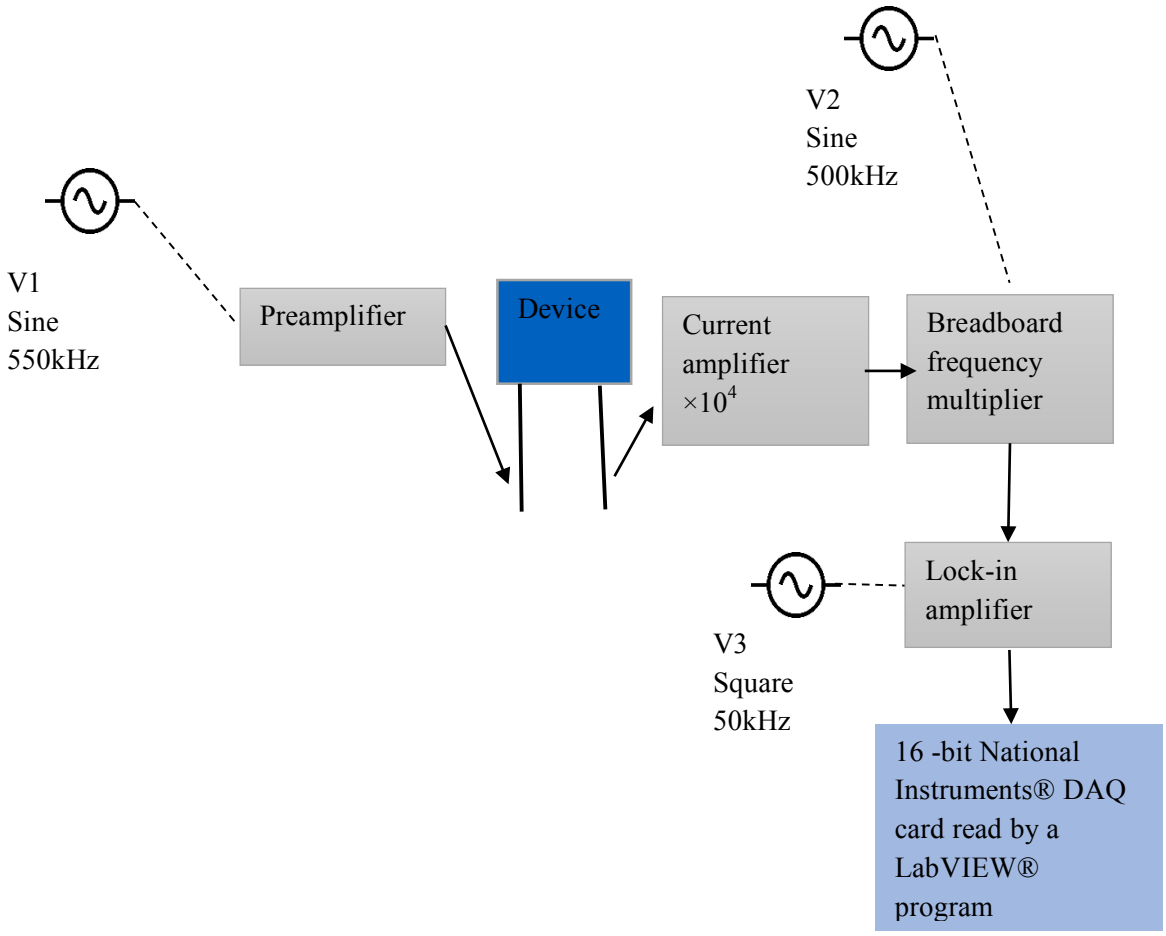

Figure 17: Overview of electronic setup used for impedance sensing. V1, V2 and V3 are function generators for the device, frequency multiplier and lock-in amplifier respectively. In this case, frequency N=500kHz.

For measurement of impedance signal, the device's chromium and gold (Cr/Au) coplanar electrodes adapted from a previous project (Riordon et al., 2014) were connected to the setup. These are an improvement over disposable and externally integrated wire electrodes, but inferior to the commercially preferred parallel facing microelectrodes. Parallel electrodes are generally considered superior, particularly due to uniformity of electric field, but are unfortunately significantly more challenging to fabricate. A similar obstacle is associated with various designs of 3-dimensional electrodes, which are considered reliable and customizable,

but often require advanced fabrication techniques and adaptation to device designs (Geng and Lu, 2013). As a result, device geometry had to take into consideration the lack of electric field uniformity by restricting channel volume. In addition, devices had to be replaced periodically after approximately one month of use (provided no other issues with the device were present), due to chemical degradation of the electrodes. Coplanar electrodes are not preferred in electroporation due to a possibility of dielecrophoretic phenomena appearing at higher voltages, where the cells might be attracted to the electrode (Pethig, 2010). In our case, voltage applied to electrodes was kept below at 0.3V to prevent membrane damage (Chang and Reese, 1990). Signal was acquired in the form of Voltage at 1kHz sampling rate through a LabView program, and post-processed in MATLAB 2016A (Mathworks). Further parameter settings are given in Table 3.

Table 3: Parameter setting for impedance sensing

Parameter	**Setting**
Function generator A	500kHz, 0.3V
Function generator B	550kHz, 0.6V
Function generator C	50kHz, 1V
Lock-in	50kHz
Amplification	10^4 amplifier, 10^1 lock-in, 10^1 unit conversion
Sampling frequency	1kHz
Central square channel side length	(40±1)μm
Inter-electrode distance (Cr/Au)	(20±1)μm
Solution	900μL cells in Dulbecco's Modified Eagle's Medium (DMEM), 90μL 2mM KCl, 10μL bovine serum albumin (BSA) stock
Initial cell concentration	$(6\pm1)\times10^6$/mL
Cell type and diameter	3T3, (18±2)μm

The frequency multiplier circuit, shown in Figure 18, was composed and used to permit operating at higher input frequencies (which allow more determinant detection of signal

differences between damaged and healthy cells), while remaining in the operating range of the lock-in amplifier (Cerda, 2013).

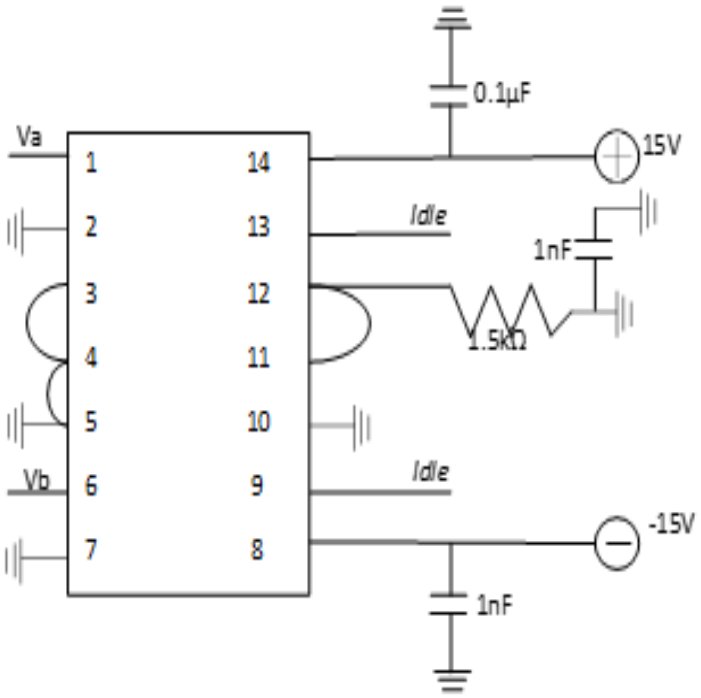

Figure 18: A schematic representation of frequency multiplier chip AD734 from Analog devices, and corresponding connections on breadboard (AD734 Datasheet and Product Info, 2016). V_a is the input (V2 in Figure 17) and V_b is the output (V3 in Figure 17).

The corresponding frequency multiplication obtained at the output is described in Equation 6 and expanded into Equation 7:

$$\left(A \sin\left(\frac{2\pi}{a}\right)\right) \times \left(B \sin\left(\frac{2\pi}{b}\right)\right) \qquad 6$$

In Equation 6, terms A and B represent amplitudes of function generators V2 and V3 (shown in Figure 10) respectively, and *a* and *b* represent their corresponding frequencies. Expanding Equation 6 provides Equation 7 below:

$$\frac{1}{2}AB(\sin\left(\frac{2\pi}{a}+\frac{2\pi}{b}\right)+\sin(\frac{2\pi}{a}-\frac{2\pi}{b})) \quad 7$$

Here, the effects of the first, additive part of the equation are removed by a low pass filter.

2.2.3 Impedance Sensing

Prior to performing experiments with cells, device and signal acquisition quality was assessed by flowing ionic solutions through the channels, followed by testing the responsiveness to flow of polystyrene microbeads with a diameter of 9μm. Cells and polystyrene microbeads were run through the device suspended in DMEM, with 1% BSA to prevent sticking and settling of cells, and 9% 2mM KCl ionic solution to improve signal observation.

Signal processed through the previously described electronic setup was acquired using a LabView program composed to measure the voltage signal at 1kHz, automatically saved to a text file. Further filtering and processing was done in MATLAB, where the valid data was subsequently summarized and visually presented.

2.2.3.1 Frequency Selection

Frequencies of input function generators were selected experimentally after testing the signal of a passing cell at twelve different frequencies to determine an ideal compromise in signal to noise ratio (SNR) and ability to distinguish cellular components (cytoplasm and plasma

membrane). At lower frequencies, below 100kHz, the double layer component significantly affects the signal. At AC frequencies above 10MHz, capacitive noise would begin to have a noticable effect (Gawad et al., 2004).

The AC frequency selected for good signal acquisition was 500kHz, where effects of cell damage were detectable, and the signal of a passing cell was sufficiently distinguishable from undesired electrical noise. However, it should be noted that this is also the frequency where cell size may have an increased effect on the signal (Riordon et al., 2014), particularly for healthy cells with intact cell membranes. While lower frequencies (100kHz and below) did not show major differences in cell signal between the two experimental settings, higher frequencies (MHz range) could be superior in detecting cell membrane damage, but included large amounts of noise. Additionally, frequencies exceeding 10^7 Hz ranges would not be considered informative for this purpose, as they provide mostly information on cytoplasmic conductivity changes for healthy cells (Gawad et al., 2004). It should be emphasized that unlike in most previous work done by other groups, the cells were not damaged irreversibly in this project, and in some cases may heal by the time they reach the electrodes for measurement.

2.3 Integration of Transfection With Impedance Sensing

2.3.1 Designs

When integrating transfection with impedance sensing, the primary concerns were finding the appropriate method of fabrication, verifying the retention of transfection efficiency, adapting pressure settings, and defining appropriate transition dimensions.

According to previous work, transient pores in 3T3 cell membranes require up to 30 seconds to heal (Sharei et al., 2014) (McNeil and Steinhardt, 2003), so distance from the final constriction to the electrodes in the impedance measurement device must enable detection and electrical measurement of a transiently porated cell within this timeframe at the appropriate flow rate (Sharei et al., 2014). The electrodes were placed as near as fabrication would permit to the final barrier feature for transfection to allow sufficient freedom in flow rate adaptation. The device design in shown in Figure 19.

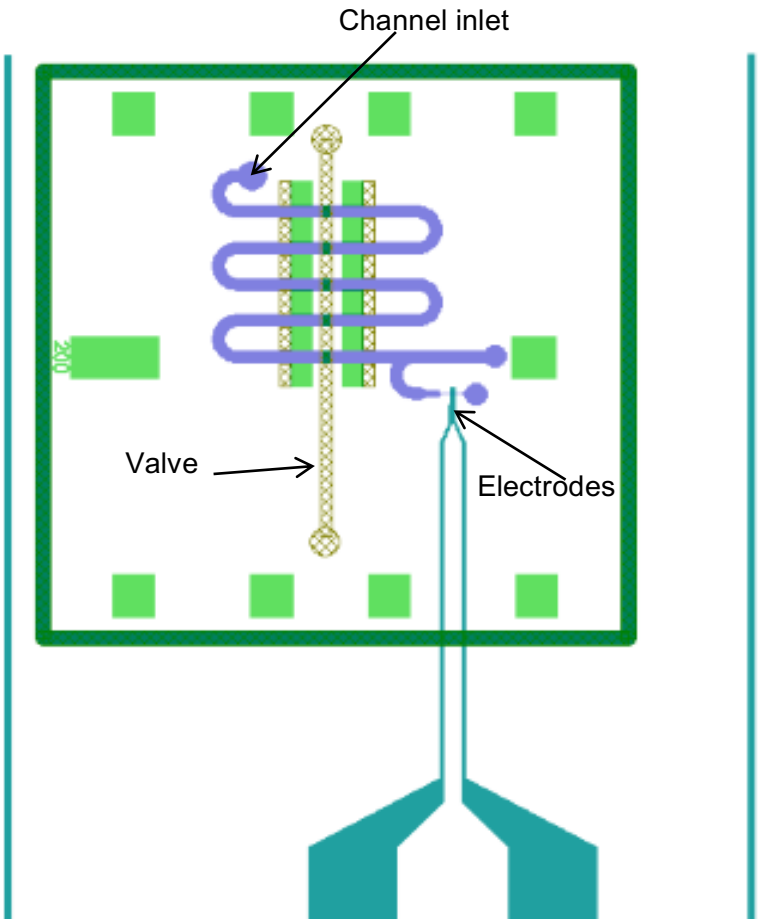

Figure 19: CleWin4 design for combined transfection and impedance sensing. Stamp, valve and channel layer are overlapping. The channel is shown in purple, the valve in yellow, and the stamp in green, while the larger, electrode layer is shown in turquoise. Details for the electrode designs are described later and in Figure 15.

*2.3.*2 Microfabrication of impedance sensing devices

While push-up valve devices are simpler to combine with impedance sensing, it was shown that their efficiency in cell transfection is inferior. Barrier-valve devices required some modification in order to be combined with impedance sensing.

For combining barrier-valve designs for microfluidic transfection and impedance sensing, a modified soft lithography technique was also tested. Following electrode fabrication, the

channel layer was created using negative photoresist deposition directly onto the glass slide with the electrodes. As in the original transfection devices, the barrier feature surface was deactivated using brief PDMS contact with a PDMS-fabricated stamp. The valve layer was fabricated using standard PDMS molding with an SU-8 mold as described previously. Bonding of the channel and valve layers was achieved with nitrogen plasma bonding as described by (Zhang et al., 2009) and (Zhang et al., 2011) (Permanent Epoxy Negative Photoresist - MicroChem 2016). However, several quality and durability issues were encountered in attempting this method, particularly in the form of SU-8 peeling from glass, despite vigorous cleaning and careful deposition. Furthermore, SU-8 photoresist would not be possible to use in medical and long-term research application due to biocompatibility risks of the material.

The final chosen fabrication was to create a four-layer PDMS device, which included an additional punched hole acting as a vertical channel connecting the transfection device channel layer to the electrodes on the glass slide through the valve layer, was designed and fabricated, and shown in Figure 20, to provide sufficient evidence that combining transfection and impedance sensing of 3T3 cells in one device is possible. The final device provided more challenges for assembly, pressure control and maintenance.

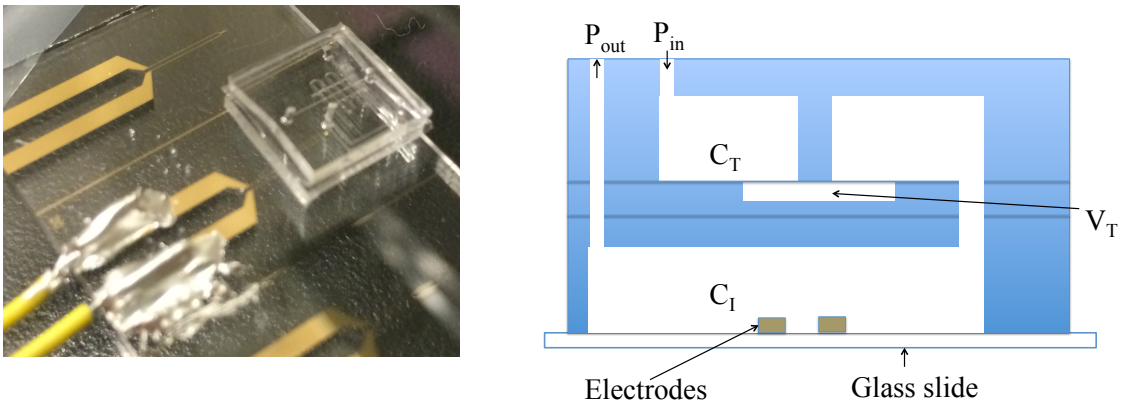

Figure 20: Successful 3-PDMS-layer device with wires already attached to electrodes on a glass slide. On the left is shown its simplified, not to scale schematic representation for the purpose of understanding the layers. 3 layers of PDMS are used. The layers from top to bottom are as follows: transfection channel layer (C_T), thin transfection valve layer (V_T), impedance measurement channel layer (C_I), gold electrodes, glass slide. Wires are shown attached with silver epoxy adhesive mixture. Only the vertical, main input P_{in} and main output P_{out} punched holes are shown.

2.3.3 Combining Process of Transfection With Impedance Sensing

Efficiency and viability results for transfection were repeated successfully with the new devices, to confirm the function of the transfection section of the device approximately matched that of the independent transfection device. While methods used for each device section independently were a good reference for parameters to use in the combined device, some aspects required minor modification. Flow and pressure settings had to be adapted for the new geometry.

Using the pressure regulators, the flow speed of cells (and microspheres) through the main microfluidic channel of the device was set at (10±1)µm/s for the first part of the device (used for transfection), and (20±5)µm/s for the second part of the device (used for impedance

sensing), with overall flow rate estimated at (100±10)μL/h. This allowed the cells to reach the electrodes in less than 30 seconds of being transfected/damaged by the barriers, while maintaining similar parameters to previous stand-alone sections.

3 Results

Results were first collected and presented separately for each of the two device functions, i.e. for efficiency and viability achieved by the transfection device, and to check what information could be gained with the impedance sensing setup with available resources. Once satisfactory function was shown for each section, the two aspects were combined into one device, where appropriate modifications were made to account for the effect of integration (such as pressure settings for flow rate, suspension media composition, and method of collection and data analysis).

3.1 Transfection

The first section of the device was aimed at transfection of cells. Results are presented for the barrier-valve design, which was later integrated with impedance measurement. Transfection experiments involved obtaining information on how the extent of constriction (length, height, and number of constricted spaces the cells passed) affected the efficiency of transfection and viability of cells. Efficiency of transfection was defined as the percentage of cells fluorescing green with FITC, while viability was defined as percentage of cells not fluorescing red with PI. Outlines of cells were defined using ImageJ, and fluorescence was identified if the cell reached a threshold of fluorescence higher than the background average.

Cells that were not viable were not included in the count for transfection efficiency.

It should be noted that in analyzing images for transfection efficiency based on fluorescence, samples and plate regions that were checked later in the set may have began to lose fluorescence. There were also minor issues in assessing the number of fluorescing cells in the presence of clumps. Fluorescence appeared to accumulate between clumped cells, making counting of FITC-labelled dextran containing cells questionable. While effort was made to avoid clump formation, some cases still appeared. Counting regions containing clumps were excluded from analysis.

Firstly, the effect of constriction dimensions for a single constriction was checked. A wide range of valve pressures and channel dimensions was explored without significant viability loss. A significant drop in viability was observed only at very high flow rates and very narrow constrictions (as narrow as 2μm). In the case of a single constriction, the best results in terms of device reliability, transfection efficiency and cell viability were obtained using a 40μm constriction length (width of the barrier), and flow rates of (20±5)μL/min. Cell viability would remain (95±5)% if the cells were not compressed below 9μm. These barrier dimensions were found to successfully transfect cells. And example is shown in Figure 21.

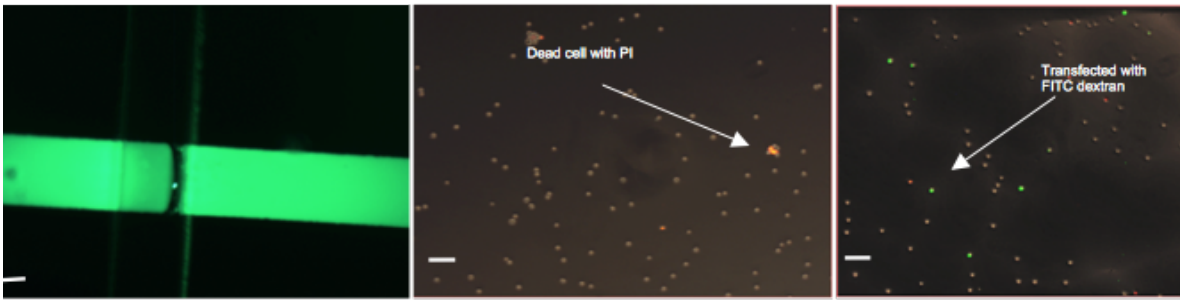

Figure 21: 3T3 cells 2 hours after being run through 40µm barrier device, rinsed and plated. The images are taken under a fluorescent lamp. The first image shows the channel filled with cells in their FITC-labelled dextran solution. Cells glowing green have been "transfected" with the 3-5kDa FITC-labelled dextran. Cells stained red with PI are no longer viable. The scale bar represents 50µm.

Compressing the cells to below 2µm caused severe damage to the cell, usually tearing and destroying it entirely as it passed the constriction, as shown in Figure 22.

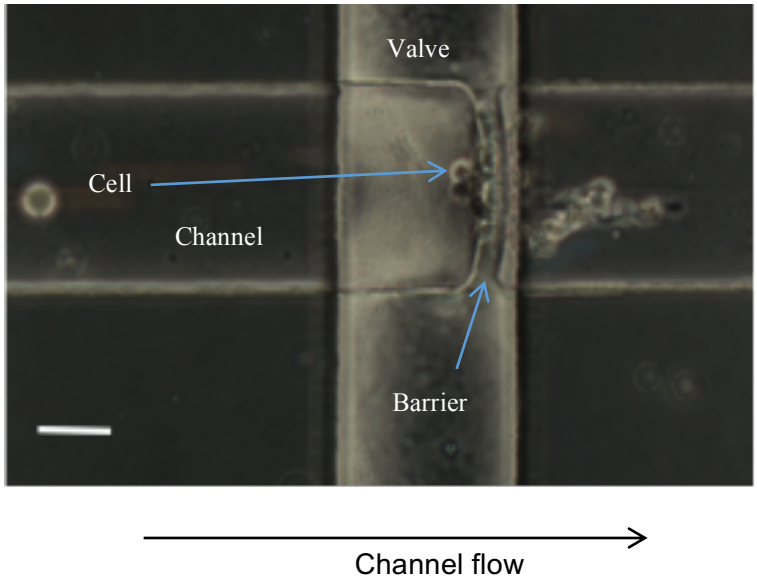

Figure 22: When the valve is highly pressurized, cells are overly constricted as they squeeze through the gap underneath the barrier, causing irreversible damage. This occurs due to the high flow rate and consequentially increased shear force on the cells. The scale bar represents 100µm.

As was done in most previous work by Sharei et al., multiple constriction devices were also fabricated and tested to compare transfection efficiency. Efficiency was significantly improved from (10±5)% for single 20μm constriction to (68±5)% for five 20μm constrictions. Figure 23 shows an example of a fluorescent image on a sample of transfected cells, taken 2 hours after transfection using the device; this permitted sufficient time for healing and partial settling of cells for improved image acquisition.

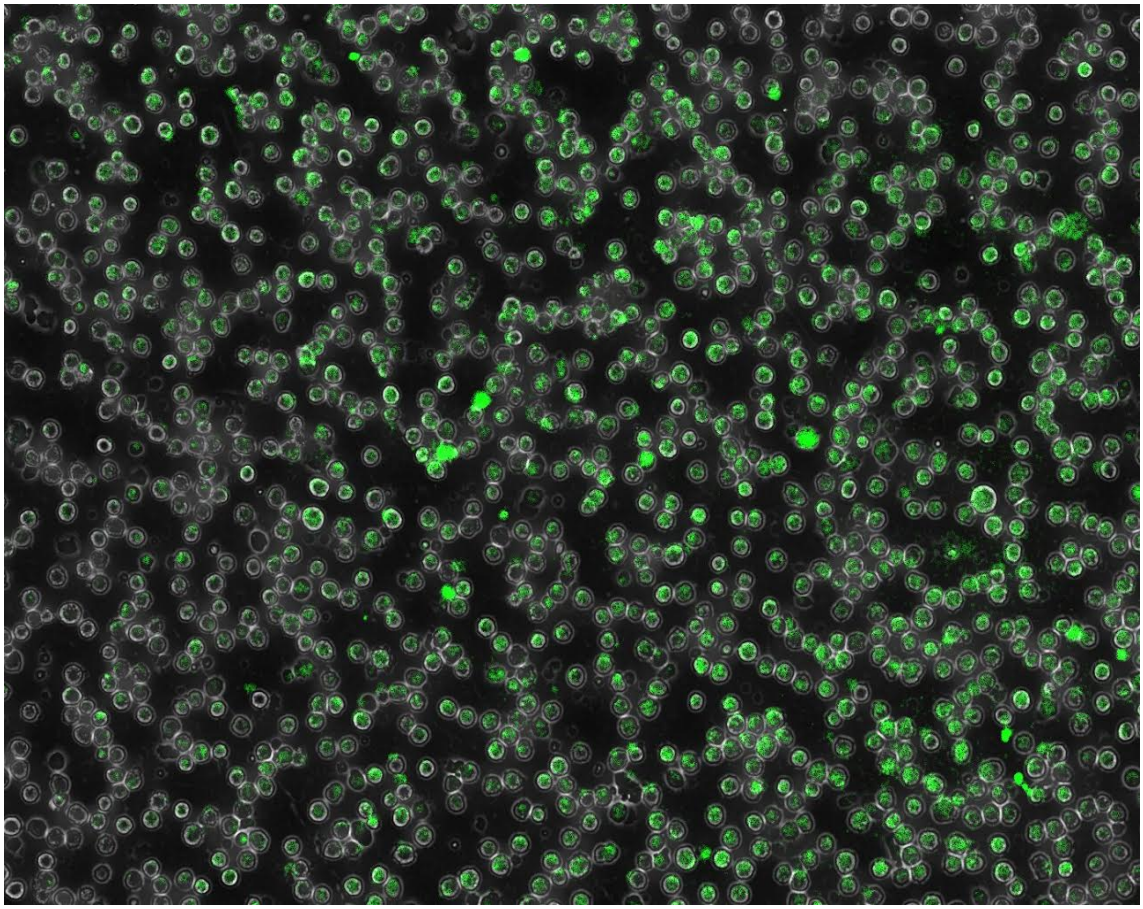

Figure 23: 3T3 cells 2 hours after being run through 5 x 20μm constriction device, rinsed and plated. Cells glowing green have been "transfected" with the 3-5kDa FITC-labelled dextran, indicating success of the procedure. Almost no cells stained red at the addition of PI, indicating near 100% viability.

An additional test of viability was performed to check if transfected cells would maintain

viability in the long term. Transfected cells were still viable after 48h of post-treatment incubation. Although cell division has already extensively taken place, it is still visible that the cells that had been transfected continue to show fluorescent signal in Figure 24.

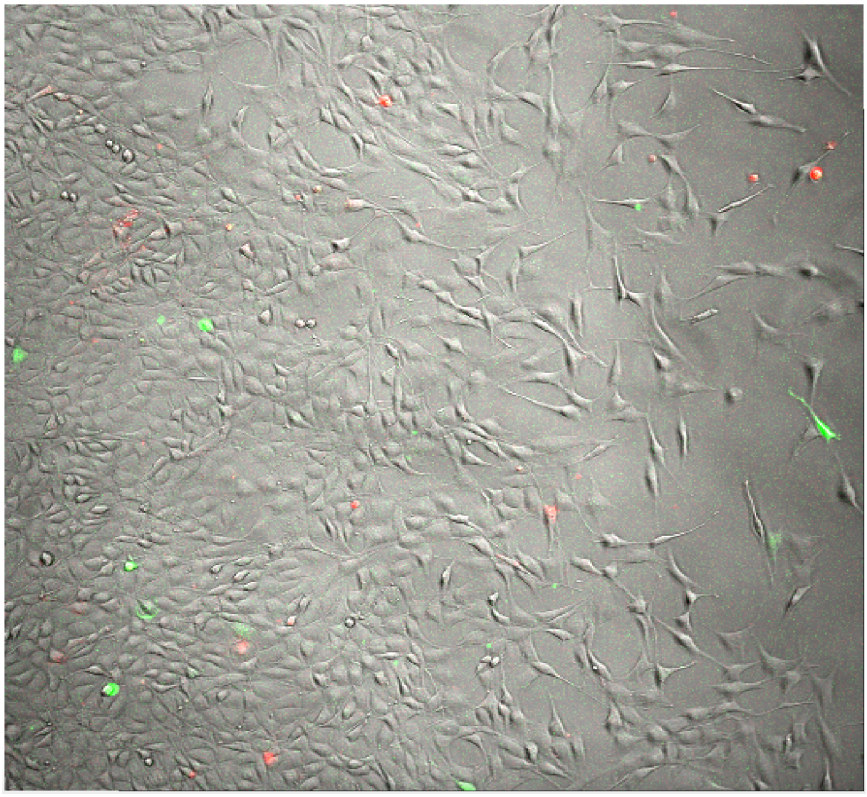

Figure 24: 3T3 cells that were run through device imaged with a confocal microscope two days after treatment and plating. Cells stained red with PI have lost viability. Cells glowing green remained "transfected" with the 3-5kDa FITC-labelled dextran. This is to show that the transfected molecules stay in the cells even days after the transfection took place.

These experiments showed that several narrower constrictions gave the best combination of viability and efficiency, and were thus in accordance with previous results (Sharei et al., 2013). Figure 25 gives a summarized comparison of efficiency and viability with different methods of transfection, as well as a control in which cells were simply left in a solution of 3kDa FITC-

labelled dextran to exclude the possibility of endocytosis. The total sample size of all trials used to estimate transfection efficiency and cell viability was 10^3 cells.

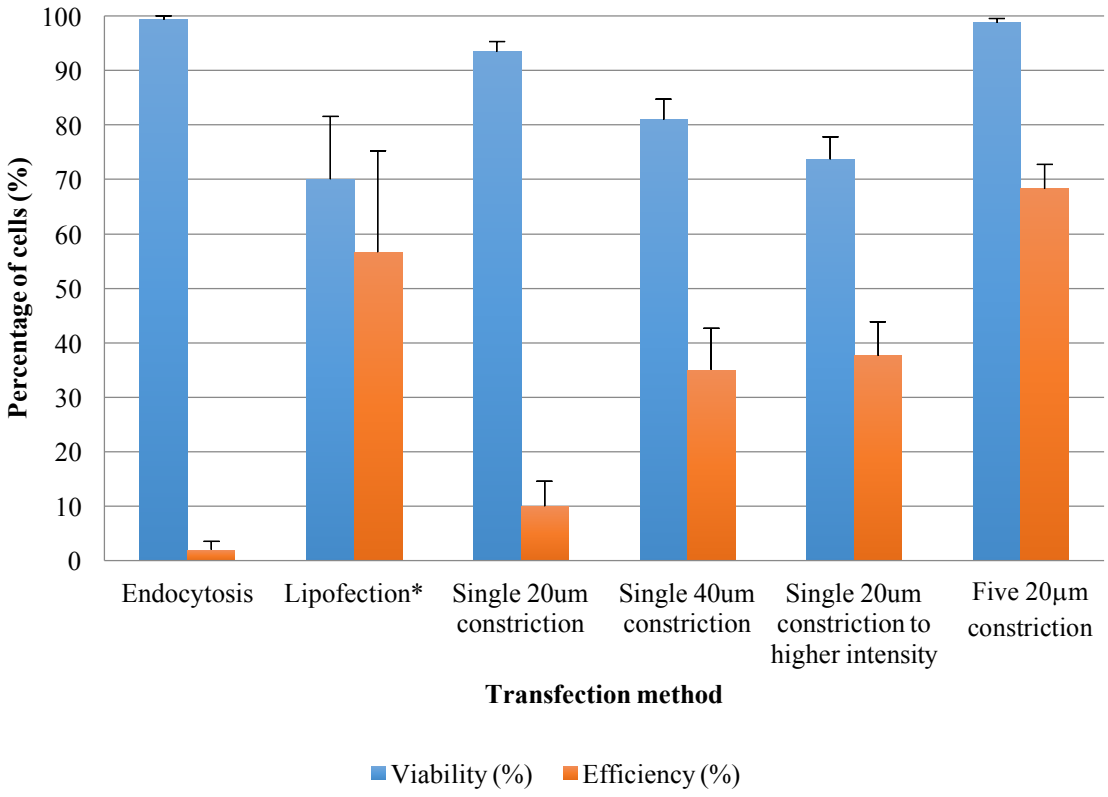

Figure 25: Efficiency of transfecting 3T3s with FITC-labelled dextran using various methods. In the case of lipofection, the plasmid PLC-delta was used instead of FITC-labelled dextran. Error bars for 2SE (five-trial based) on independent samples. Experiments had ten replicates (samples counted from same test) and five independent samples (tests performed). *For lipofection, a green fluorescent protein plasmid is used instead of FITC-labelled dextran, as is the standard of the procedure.

From these results, it is deduced that in this experimental setup, the five 20µm long constrictions were the most efficient in transfecting cells and maintaining viability, having transfected (68±5)% of the analyzed cells and maintained (99±1)% viability. Therefore, this design was later used for integration with impedance sensing.

3.2 Electrical Impedance Sensing

The second function of the microfluidic device was impedance sensing of cells. It was first necessary to test the ability of the device and its corresponding setup to measure the impedance of a passing cell. As explained in earlier sections, a passing cell created a voltage drop corresponding to a change in measured current as it passed the electrode pair. An example of a voltage drop due to a passing cell is shown in Figure 26.

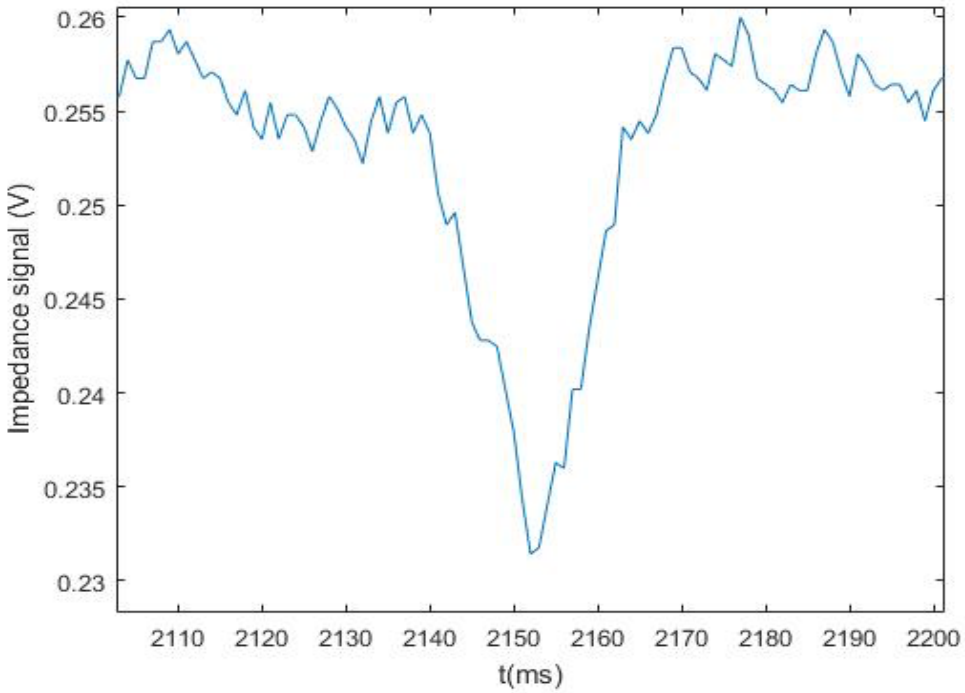

Figure 26: A voltage drop caused by a single 3T3 cells passing the electrodes of the device. The signal is a time-scale extract of impedance measurement signal (V) from a preliminary run with 3T3 cells in the experimental solution. Signal amplitude includes amplification of preamplifier, signal amplifier, and lock-in amplifier. The peak was taken from a random time point, shown in the time scale of a 10-minute test run.

Upon obtaining signals such as the one above, only the baseline-to-peak signal had to be extracted. This was done using a previously created MATLAB program. The baseline voltage signal was subtracted from the voltage amplitude of each identified peak. The signal of this

drop was amplified by a factor of 10^2 and inverted for facilitated analysis. Acquired peaks were then summarized into histograms. Figure 27 shows a histogram generated from refined, S-G filtered MATLAB peak selection with manual confirmation, from a 5-minute run in transfection solution in the combined device with no pressure on the valve.

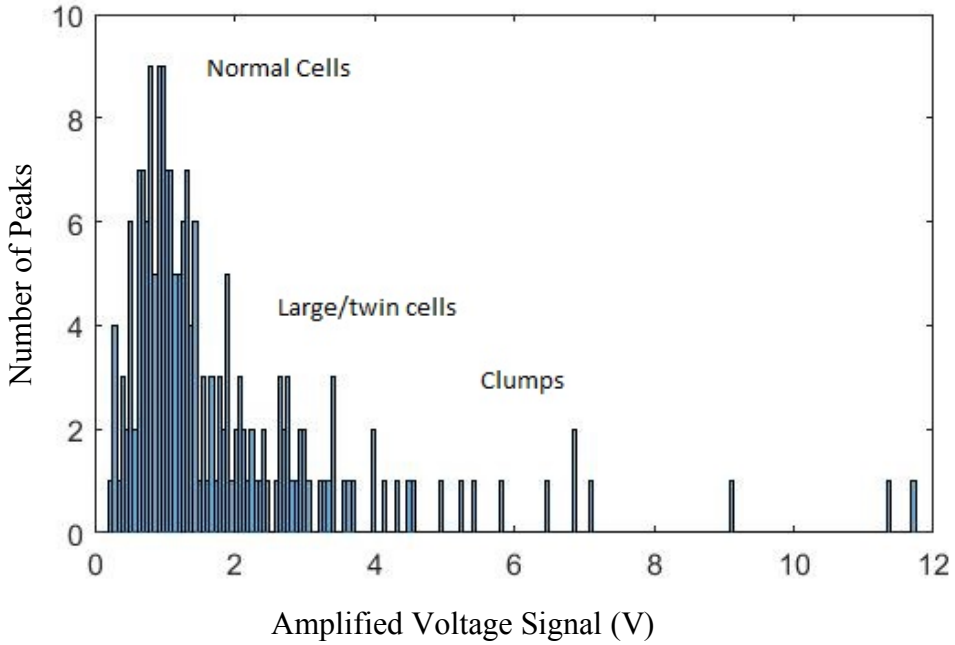

Figure 27: Example a histogram generated from refined, S-G filtered MATLAB peak selection with manual confirmation, from a 5-minute run in transfection solution in the combined device with no pressure on the valve. Signal amplitude of cells running through the uncompressed channel includes amplification of preamplifier, signal amplifier, and lock-in amplifier, as well as 10^2 post-processing amplification for facilitated MATLAB analysis. The wide range of absolute signal amplitudes, despite filtering of noise, indicates the sensitivity of the measurement system to the cell size variability.

These preliminary results confirmed the functionality of the setup for sensing impedance of passing cells. The next step is to confirm this can be combined with the cell transfection, and can be used to detect a difference in voltage signal between cells that were transfected and those that were flowing freely through the device.

3.3 Combined Transfection and Impedance Sensing

The next set of results involved comparing the transfection efficiency and impedance signal for cells that were transfected, and those that were not.

Prior to including pressure on the valve for transfection, the device was tested to check the necessary adaptations to parameters for impedance measurement, such as pressures, concentration of KCl in solution for cell suspension, and signal amplification. Calibration with beads was done at two sizes (20μm and 9μm) to re-confirm required pressures and flow rates. Dilution of dextran and settings for electronic measurement were maintained according to previous experiments for the two independent components, as described in the methods section. Viability and transfection efficiency were found to be maintained at similar values to the independent device.

The cells were either transfected (using five barriers with a constriction height of 9μm), or left to run freely through the device, and their impedance was measured by the final section of the device. Transfection efficiency and impedance signals were obtained as previously described for both conditions. Mean impedance was found from histograms as previously described. Presence of transfection was found based on whether or not the average intensity of cells was greater than the background fluorescence. Figure 28 shows a summary of FITC fluorescent intensity and impedance sensing signal for “transfected” cells, and cells run through the device without compression. Fluorescence was clearly present in the transfected cells, as fluorescent signal intensity was higher than the background intensity, and was not present in cells flowing freely. Mean peak amplitude (post-amplification) was (0.027±0.002)V for damaged cells and

(0.023±0.002)V for healthy cells. The difference of means for this experimental run was (0.004±0.002)V. However, it should be noted that sample sizes were very small for an experiment of this type (11 significant peaks for damaged cells and 76 for healthy cells), and the successful experiment is not necessarily indicative of the reliability of the method. Additional experiments are needed to confirm the results.

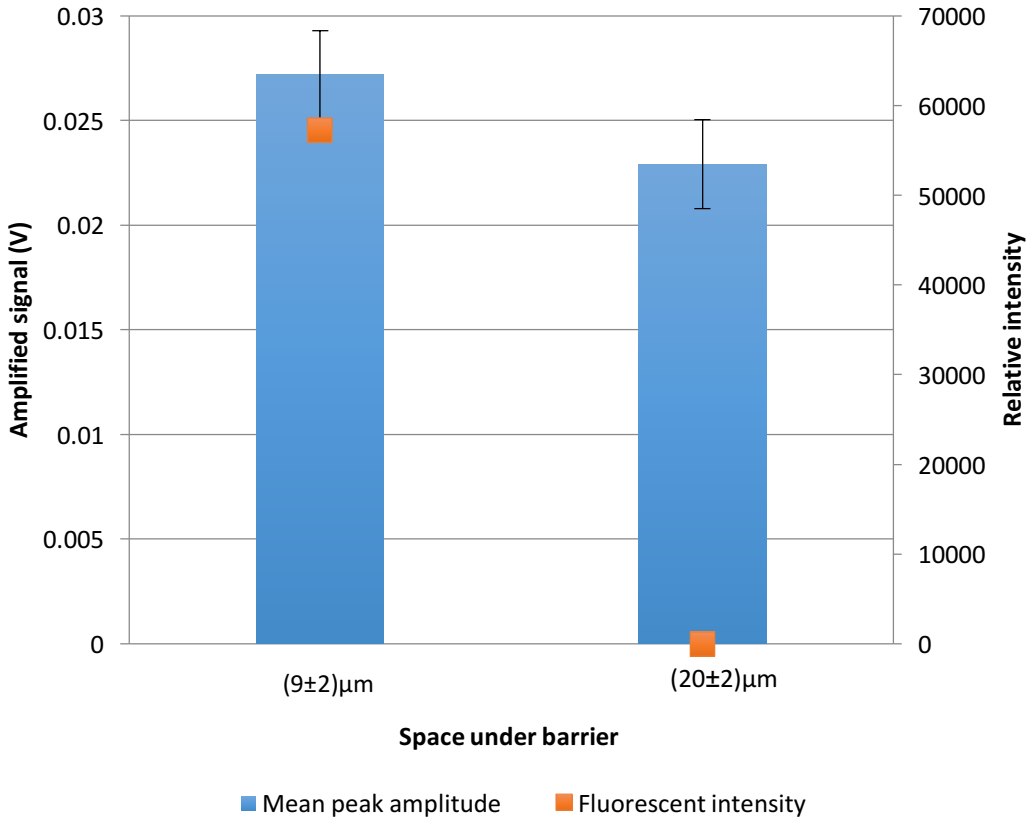

Figure 28: Voltage signal and fluorescence intensity comparison for cells compressed to (9±2)µm or allowed to flow through freely through (20±2)µm. Each sample run is analyzed independently. Sample sizes were 100 cells and less. Error bars were caused by the effect of size variability on the signal. Intensity of fluorescent signal as a result of transfection was nominally compared at this stage and found to be clearly distinguishable between the treated and untreated sample

4 Summary and Further Steps

4.1 Summary and Interpretation of Results

As seen from the results, it is possible to insert small, 3kDa molecules into 3T3 cells by applying shear stress to them using controllable constrictions in the microfluidic device described. By adding an impedance sensing component as a section of the device, we may eventually be able to identify the approximate degree of constriction when cells begin to undergo damage, permitting small molecules to enter the cells. It has been shown that the current setup for measurement of impedance can be used to assess cell damage in the form of membrane poration to some extent, provided that cell damage is clearly identifiable and impedance is measured within a few seconds of damage. At this stage, this is possible by checking a number of cells sufficient for statistical assessment of differences in the signal.

Unfortunately, it is difficult to define the precise point when a cell becomes transiently porated. As described in earlier chapters, previous work has been able to note the difference between a single healthy cell and a single electroporated and non-viable cell, but did not compare various extents of reversible membrane damage, or the change in signal for a damage cell that is still capable of recovery. Improvement to design and setup equipment may permit progress in the direction of step-wise identification of changes in transfection efficiency in relation to various parameters (such as constriction extent and flow rate) through comparison of impedance measurement and fluorescence intensity. If developed, this method may reduce the need for extensive trial-and-error calibration for every cell type, since the point of poration can be identified on-chip while the device is running. It should be noted that cell concentration would be lower post-treatment due to losses associated with clogging in the device, rinsing

and transferring. Similarly to previous work, it was found that increasing the number of times the cells are constricted is more efficient that increasing the length of constriction, and also allows for operation at lower flow rates, resulting in a reduced cell and viability loss.

4.2 Future Work

The current devices, as described in this work, were fabricated using available methods and resources. In a commercial device, it would be desirable to have parallel facing electrodes rather than coplanar electrodes in order to improve quality of signal acquisition. It would also be beneficial to include multiple frequency impedance analysis. In combination, these modifications would likely improve sensitivity, reduce effects of electric field, account for size scattering and provide for more detailed insights. Furthermore, by adding systems to distinguish components of impedance, it may be possible to simultaneously track events resulting in cell death (Gou et al., 2011). Further steps may include more efficient and step-wise analysis of the extent of membrane damage on-chip, potential addition of post-transfection treatment (such as microfluidic-assisted encapsulation), as well as adding additional transfection material inputs to enhance the utility (a method of mixing would also be incorporated (Lee, Chang, Wang, and Fu, 2011). Currently, 3kDa molecules were used to replicate DNA; larger, 70kDa molecules could eventually be used to test efficiency at protein size level. A flow-cytometry analysis of fluorescence (FACS) may also yield more informative results on transfection efficiency. Eventually, stem cell and more complex and functional transfection molecules should be used, as this would permit us to work towards confirming that the device is capable of fulfilling the purpose for which it was initially developed to a superior level in comparison to previous methods.

5 Conclusion

In this work, a new method of microfluidic mammalian cell membrane poration using shear stress was combined with on-chip impedance sensing in an attempt to combine transfection and cell membrane integrity assessment on a single device and corresponding setup. It was shown that using a set of experimentally determined parameters, cell transfection efficiency of (68±5)% can be reached with small, 3kDa molecules, while maintaining viability of (95±5)%. Due to challenges with regards to sensitivity, impedance measurements were less determinant. Nevertheless, it was possible to monitor passing cells at a frequency of 1000Hz, with subsequent statistical analysis of sets of approximately 100 cells showing a visible difference in the signal amplitude of passing untreated versus damaged (and subsequently transfected) cells.

Due to external effects on FITC fluorescence intensity of individual cells, transfection efficiency was first determined based on fraction of cells transfected rather than comparison of intensity. Differences in cell impedance between intact and porated cells were assessed based on average values from large data sets. As the signal is affected by several other factors in addition to membrane integrity, particularly small differences in cell size and proximity to coplanar electrodes, only two parameter settings, intact cells and predetermined setting for cell transfection, were compared.

Due to its novelty, the device can continue to be modified and improved in several aspects, in terms of quality and added function. Upon availability, the possibility of using parallel facing electrodes and analysis at multiple frequencies simultaneously may significantly increase

amount of information obtainable from results. Direct deposit of impedance analysis channel layer may also be explored to allow more precise control over channel dimensions and fabrication success rate.

Functionality may also be added to the current device, such as an already existing cell cocooning module for encapsulation of successfully transfected cells, and input of multiple transfection material. Despite being set in preliminary stages at this point, a major hurdle showing promising results in functionality and potential has been overcome in the described work, setting a good starting point for further progression of a less-explored method of transfection and a corresponding new device.

References

1. About Lock-In Amplifiers. (n.d.). Retrieved August 8, 2016, from http://www.thinksrs.com/downloads/PDFs/ApplicationNotes/AboutLIAs.pdf
2. AD734 Datasheet and Product Info. (n.d.). Retrieved August 08, 2016, from http://www.analog.com/en/products/linear-products/analog-multipliers-dividers/ad734.html
3. Alrifaiy, A., Lindahl, O., and Ramser, K. (2012). Polymer-based microfluidic devices for pharmacy, biology and tissue engineering. Polymers, 4(3) Retrieved from http://pure.ltu.se/portal/sv/publications/polymerbased-microfluidic-devices-for-pharmacy-biology-and-tissue-engineering(3f73a5e4-7ed1-4dde-9651-b7610dcc78bc).html
4. Andrews, N. W., Almeida, P. E., and Corrotte, M. (2014). Damage control: Cellular mechanisms of plasma membrane repair. Trends in Cell Biology, 24(12), 734-742. doi:10.1016/j.tcb.2014.07.008
5. Bürgel, S. C., Escobedo, C., Haandbæk, N., and Hierlemann, A. (2015). On-chip electroporation and impedance spectroscopy of single-cells. Sensors and Actuators B: Chemical, 210, 82-90. doi:10.1016/j.snb.2014.12.016
6. Cerda, R. M. (2013, April). Frequency Multiplication Techniques. Retrieved August 9, 2016, from http://www.crystek.com/documents/appnotes/Frequency_Multiplication_Techniques.pdf
7. Chang, D. C., and Reese, T. S. (1990). Changes in membrane structure induced by electroporation as revealed by rapid-freezing electron microscopy. Biophysical

Journal, 58(1), 1-12. doi:10.1016/S0006-3495(90)82348-1

8. Chen, J., Xue, C., Zhao, Y., Chen, D., Wu, M., and Wang, J. (2015). Microfluidic impedance flow cytometry enabling high-throughput single-cell electrical property characterization. International Journal of Molecular Sciences, 16(5), 9804-9830. doi:10.3390/ijms16059804
9. Cheung, K. C., Di Berardino, M., Schade-Kampmann, G., Hebeisen, M., Pierzchalski, A., Bocsi, J.,. .. Tárnok, A. (2010). Microfluidic impedance-based flow cytometry. Cytometry Part A, 77A(7), 648-666. doi:10.1002/cyto.a.20910
10. Chokkalingam, V., Weidenhof, B., Krämer, M., Maier, W. F., Herminghaus, S., and Seemann, R. (2010). Optimized droplet-based microfluidics scheme for sol-gel reactions. Lab on a Chip, 10(13), 1700. doi:10.1039/b926976b
11. Clausen, C. H., Skands, G. E., Bertelsen, C. V., and Svendsen, W. E. (2014). Coplanar electrode layout optimized for increased sensitivity for electrical impedance spectroscopy. Micromachines, 6(1), 110-120. doi:10.3390/mi6010110
12. Coster, H. G. L., Chilcott, T. C., and Coster, A. C. F. (1996). Impedance spectroscopy of interfaces, membranes and ultrastructures. Bioelectrochemistry and Bioenergetics, 40(2), 79-98. doi:10.1016/0302-4598(96)05064-7
13. Das, A. K., Gupta, P., and Chakraborty, D. (2015). Physical methods of gene transfer: Kinetics of gene delivery into cells: A review. Agricultural Reviews, 36(1), 61-66. doi:10.5958/0976-0741.2015.00007.0
14. Dittrich, P. S., and Manz, A. (2006). Lab-on-a-chip: Microfluidics in drug discovery. Nature Reviews. Drug Discovery, 5(3), 210-218. doi:10.1038/nrd1985
15. Djakov, T., Popovic, I., and Rajakovic, L. (2014). Micro-electro-mechanical systems (MEMS): Technology for the 21st century. Hemijska Industrija, 68(5), 629-641.

doi:10.2298/HEMIND131008091D

16. Fink, S. L., and Cookson, B. T. (2005). Apoptosis, pyroptosis, and necrosis: Mechanistic description of dead and dying eukaryotic cells. Infection and Immunity, 73(4), 1907-1916. doi:10.1128/IAI.73.4.1907-1916.2005
17. Fluorescence Fundamentals. (2015). Retrieved August 08, 2016, from https://www.thermofisher.com/si/en/home/references/molecular-probes-the-handbook/introduction-to-fluorescence-techniques.html
18. Fritzsch, F. S. O., Dusny, C., Frick, O., and Schmid, A. (2012). Single-cell analysis in biotechnology, systems biology, and Biocatalysis. Annual Review of Chemical and Biomolecular Engineering, 3(1), 129–155. doi:10.1146/annurev-chembioeng-062011-081056
19. Gawad, S., Cheung, K., Seger, U., Bertsch, A., and Renaud, P. (2004). Dielectric spectroscopy in a micromachined flow cytometer: Theoretical and practical considerations. Lab on a Chip, 4(3), 241-251. doi:10.1039/b313761a
20. Geng, T., and Lu, C. (2013). Microfluidic electroporation for cellular analysis and delivery. Lab Chip, 13(19), 3803–3821. doi:10.1039/c3lc50566a
21. Gou, H., Zhang, X., Bao, N., Xu, J., Xia, X., and Chen, H. (2011). Label-free electrical discrimination of cells at normal, apoptotic and necrotic status with a microfluidic device. Journal of Chromatography. A, 1218(33), 5725-5729. doi:10.1016/j.chroma.2011.06.102
22. Granton, J., Langleben, D., Kutryk, M. B., Camack, N., Galipeau, J., Courtman, D. W., and Stewart, D. J. (2015). Endothelial NO-synthase gene-enhanced progenitor cell therapy for pulmonary arterial hypertension: The PHACeT trial. Circulation Research, 117(7), 645-654. doi:10.1161/CIRCRESAHA.114.305951

23. Harris, J., Lee, H., Vahidi, B., Tu, C., Cribbs, D., Jeon, N. L., and Cotman, C. (2007). Fabrication of a microfluidic device for the compartmentalization of neuron soma and axons. Journal of Visualized Experiments : JoVE, (7) doi:10.3791/261

24. Hesketh, P. J. (1998). Proceedings of the symposium on microstructures and microfabricated systems IV. Paper presented at the, 1998,14

25. Hinkeldey, B., Schmitt, A., and Jung, G. (2008). Comparative photostability studies of BODIPY and fluorescein dyes by using fluorescence correlation spectroscopy. Chemphyschem : A European Journal of Chemical Physics and Physical Chemistry, 9(14), 2019-2027. doi:10.1002/cphc.200800299

26. Iliescu, C., Taylor, H., Avram, M., Miao, J., and Franssila, S. (2012). A practical guide for the fabrication of microfluidic devices using glass and silicon. Biomicrofluidics, 6(1), 016505–016505–16. http://doi.org/10.1063/1.3689939

27. Jinturkar, K. A., Rathi, M. N., and Misra, A. (2011). 3 - gene delivery using physical methods. In A. Misra (Ed.), Challenges in delivery of therapeutic genomics and proteomics (pp. 83-126). London: Elsevier. doi://dx.doi.org/10.1016/B978-0-12-384964-9.00003-7

28. Johnson, I. (2010). *The molecular probes handbook: A guide to fluorescent probes and labeling technologies* (11th ed.). Carlsbad, CA: Life Technologies Corporation.

29. Kim, J. S. (2008). Research highlights. Nanomedicine, 3(6), 757. doi:10.2217/17435889.3.6.757

30. Kollmannsperger, A., Sharei, A., Raulf, A., Heilemann, M., Langer, R., Jensen, K. F., Tampé, R. (2016). Live-cell protein labelling with nanometre precision by cell squeezing. Nature Communications, 7, 10372. doi:10.1038/ncomms10372

31. Kovarik, M. L., Ornoff, D. M., Melvin, A. T., Dobes, N. C., Wang, Y., Dickinson, A.

J., Allbritton, N. L. (2013). Micro total analysis systems: Fundamental advances and applications in the laboratory, clinic, and field. Analytical Chemistry, 85(2), 451-472. doi:10.1021/ac3031543

32. Kurz, C. M., Büth, H., and Thielecke, H. (2010). Influence of transfection process on single cell impedance. Journal of Physics: Conference Series, 224(1), 012082. doi:10.1088/1742-6596/224/1/012082
33. Kwapiszewska, G., Hoffmann, J., Kovacs, G., Stacher, E., Olschewski, A., and Olschewski, H. (2016). [Pulmonary arterial hypertension]. Pneumologie (Stuttgart, Germany), doi:10.1055/s-0042-100537
34. Lake, M., Narciso, C., Cowdrick, K., Storey, T., Zhang, S., Zartman, J., and Hoelzle, D. (2015). Microfluidic device design, fabrication, and testing protocols. Protocol Exchange. doi:10.1038/protex.2015.069
35. Laurell, T., and Lenshof, A. (2015). *Microscale Acoustofluidics*. (pp. 46-64). Cambridge: Royal Society of Chemistry.
36. Lecoeur, H. (2002). Nuclear apoptosis detection by flow cytometry: Influence of endogenous endonucleases. Experimental Cell Research, 277(1), 1-14. doi:10.1006/excr.2002.5537
37. Mansor, M. A., and Ahmad, M. R. (2015). Single cell electrical characterization techniques. International Journal of Molecular Sciences, 16(6), 12686-12712. doi:10.3390/ijms160612686
38. Martel, J. M., and Toner, M. (2014). Inertial Focusing in Microfluidics. *Annual Review of Biomedical Engineering Annu. Rev. Biomed. Eng., 16*(1), 371-396. doi:10.1146/annurev-bioeng-121813-120704
39. Marx, V. (2016). Cell biology: Delivering tough cargo into cells. Nature Methods,

13(1), 37-40. doi:10.1038/nmeth.3693

40. Microinjection : Methods and applications / edited by David J. carroll (2009).. New York: Humana Press.
41. Mosadegh, B., Takayama, S., Tung, Y., Bersano-Begey, T., Tavana, H., Kuo, C., and Torisawa, Y. (2010). Integrated elastomeric components for autonomous regulation of sequential and oscillatory flow switching in microfluidic devices. Nature Physics, 6(6), 433-437. doi:10.1038/nphys1637
42. Otto-Wilhelm Merten, M. A. (2011). Viral vectors for gene therapy: Methods and protocols. New York, New York (State): Humana Press.
43. Permanent Epoxy Negative Photoresist - MicroChem. (2016). Retrieved August 8, 2016, from http://microchem.com/pdf/SU-82000DataSheet2025thru2075Ver4.pdf
44. Pethig, R. (2010). Dielectrophoresis: Status of the theory, technology, and applications. Biomicrofluidics, 4(2), 022811. doi:10.1063/1.3456626
45. Pierzchalski, A., Hebeisen, M., Mittag, A., Di Berardino, M., and Tarnok, A. (2010). Label-free single cell analysis with a chip-based impedance flow cytometer. Paper presented at the, 7568 11. doi:10.1117/12.840865
46. Promega. (2016). Transfection. Retrieved from http://www.promega.ca/resources/product-guides-and-selectors/protocols-and-applications-guide/transfection/
47. Riordon, J., Nash, M., Calderini, M., and Godin, M. (2014). Using active microfluidic flow focusing to sort particles and cells based on high-resolution volume measurements. Microelectronic Engineering, 118, 35–40. doi:10.1016/j.mee.2014.02.003
48. Schantz, J., and Ng, K. W. (2005). A manual for primary human cell culture. Cell

Transplantation, 14(10), 859-860. doi:10.3727/000000005783982585

49. Segré, G., and Silberberg, A. (1961). Radial particle displacements in poiseuille flow of suspensions. Nature, 189(4760), 209-210. doi:10.1038/189209a0
50. Sharei, A., Cho, N., Mao, S., Jackson, E., Poceviciute, R., Adamo, A.,. .. Jensen, K. F. (2013). Cell squeezing as a robust, microfluidic intracellular delivery platform. Journal of Visualized Experiments : JoVE, (81) doi:10.3791/50980
51. Sharei, A., Poceviciute, R., L. Jackson, E., Cho, N., Mao, S., C. Hartoularos, G., F. Jensen, K. (2014). Plasma membrane recovery kinetics of a microfluidic intracellular delivery platform. Integrative Biology, 6(4), 470-475. doi:10.1039/C3IB40215K
52. Sharei, A., Trifonova, R., Jhunjhunwala, S., Hartoularos, G. C., Eyerman, A. T., Lytton-Jean, A., Jensen, K. F. (2015). Ex vivo cytosolic delivery of functional macromolecules to immune cells. Plos One, 10(4), e0118803. doi:10.1371/journal.pone.0118803
53. Sharei, A., Zoldan, J., Adamo, A., Sim, W. Y., Cho, N., Jackson, E., Jensen, K. F. (2013). A vector-free microfluidic platform for intracellular delivery. Proceedings of the National Academy of Sciences, 110(6), 2082-2087. doi:10.1073/pnas.1218705110
54. Song, L., Hennink, E. J., Young, I. T., and Tanke, H. J. (1995). Photobleaching kinetics of fluorescein in quantitative fluorescence microscopy. Biophysical Journal, 68(6), 2588-2600. doi:10.1016/S0006-3495(95)80442-X
55. Spence, M. T., and Johnson, I. D. (2010). The molecular probes handbook: A guide to fluorescent probes and labeling technologies. Carlsbad, CA: Life Technologies Corporation.
56. Sudowe, S. (2013). Biolistic DNA delivery. New York [u.a.]: Humana Press.

57. Sueblinvong, V., and Weiss, D. J. (2010). Stem Cells and Cell Therapy Approaches in Lung Biology and Diseases. Translational Research : The Journal of Laboratory and Clinical Medicine, 156(3), 188–205. http://doi.org/10.1016/j.trsl.2010.06.007

58. Sun, T., and Morgan, H. (2010). Single-cell microfluidic impedance cytometry: A review. Microfluidics and Nanofluidics, 8(4), 423-443. doi:10.1007/s10404-010-0580-9

59. Teissié, J., and Rols, M. P. (1993). An experimental evaluation of the critical potential difference inducing cell membrane electropermeabilization. Biophysical Journal, 65(1), 409-413. doi:10.1016/S0006-3495(93)81052-X

60. Todaro, G. J., and Green, H. (1963). Quantitative studies of the growth of mouse embryo cells in culture and their development into established lines. The Journal of Cell Biology, 17(2), 299-313. doi:10.1083/jcb.17.2.299

61. Unger, M. A., Chou, H., Thorsen, T., Scherer, A., and Quake, S. R. (2000). Monolithic microfabricated valves and pumps by multilayer soft lithography. Science, 288(5463), 113-116. doi:10.1126/science.288.5463.113

62. Vandergriff, A. C., Hensley, T. M., Henry, E. T., Shen, D., Anthony, S., Zhang, J., and Cheng, K. (2014). Magnetic targeting of cardiosphere-derived stem cells with ferumoxytol nanoparticles for treating rats with myocardial infarction. Biomaterials, 35(30), 8528-8539. doi:10.1016/j.biomaterials.2014.06.031

63. Varkouhi, A. K., Scholte, M., Storm, G., and Haisma, H. J. (2011). Endosomal escape pathways for delivery of biologicals. Journal of Controlled Release: Official Journal of the Controlled Release Society, 151(3), 220-228. doi:10.1016/j.jconrel.2010.11.004

64. Volpatti, L. R., and Yetisen, A. K. (2014). Commercialization of microfluidic devices. Trends in Biotechnology, 32(7), 347. doi:10.1016/j.tibtech.2014.04.010

65. Wang, H., and Lu, C. (2006). Electroporation of mammalian cells in a microfluidic channel with geometric variation. Analytical Chemistry, 78(14), 5158-5164. doi:10.1021/ac060733n

66. Widengren, J., Chmyrov, A., Eggeling, C., Löfdahl, P., and Seidel, C. A. M. (2007). Strategies to improve photostabilities in ultrasensitive fluorescence spectroscopy. The Journal of Physical Chemistry. A, 111(3), 429. Retrieved from http://www.ncbi.nlm.nih.gov/pubmed/17228891

67. Wolfson, R., and Mullen, D. (2010). Spreadsheet lock-in amplifier. American Journal of Physics, 78(11), 1227-1229. doi:10.1119/1.3450178

68. Zhang, Z., Zhao, P., and Xiao, G. (2009). The fabrication of polymer microfluidic devices using a solid-to-solid interfacial polyaddition. Polymer, 50(23), 5358-5361. doi:10.1016/j.polymer.2009.09.053

69. Zhang, Z., Zhao, P., Xiao, G., Watts, B. R., and Xu, C. (2011). Sealing SU-8 microfluidic channels using PDMS. Biomicrofluidics, 5(4), 8. doi:10.1063/1.3659016

70. Zheng, Y., Shojaei-Baghini, E., Wang, C., and Sun, Y. (2013). Microfluidic characterization of specific membrane capacitance and cytoplasm conductivity of singlecells. Biosensors and Bioelectronics, 42, 496–502. doi:10.1016/j.bios.2012.10.081

71. Zhu, Z., Frey, O., Haandbaek, N., Franke, F., Ottoz,, D., Rudolf, F., and Hierlemann, A. (2012). Electrical-Impedance-Spectroscopy Characterization Of Individually Immobilized Single Particles And Yeast Cells, 16th International Conference on Miniaturized Systems for Chemistry and Life Sciences, Okinawa, Japan, October 28 - November 1, 2012

Appendix

Appendix I – Protocols

Protocols are adapted from the group website, http://openwetware.org/wiki/Godin

Piranha Etch

1. Put on a protective mask, apron and rubber gloves. Cover surface of fumehood with blue acid detection wipes. Turn on tap and leave water running.
2. Fill a 1L beaker with 200mL of water for acid waste.
3. Pour 10mL of H_2O_2 in small beaker.
4. Measure 30 mL of sulfuric acid and mix it with the H_2O_2 in a glass flat bottom dish.
5. Blow dry a silicon wafer and gently place it in the piranha solution.
6. Shake the acid bath gently at the start and after 15 minutes.
7. After 30 minutes, transfer the wafer(s) into a clean glass dish filled with water, repeat 3 times.
8. Rinse all containers thoroughly. Empty the acid in the waste beaker and let it degas through the night.

Cell Splitting

1. Wear a lab coat and nitrile gloves. Spray everything that enters the biological cabinet with 70 % ethanol.
2. Heat DMEM culture medium (10% foetal bovine albumin and 1% penicillin/streptomycin) and trypsin (0.05 %) to 37°C.
3. Under a biological cabinet, remove the culture medium from the culture dish and add 10mL of phosphate buffered saline (PBS).
6. Remove the PBS and add 5mL of trypsin; incubate until cells detach, approximately 3 minutes
7. Add 5 mL of culture medium and transfer the cell suspension to a 15mL falcon tube. Centrifuge at 1000 rotations per minute, for 3 minutes.
8. Remove the supernatant, and resuspend the cells in 1-5mL of DMEM culture medium, as appropriate for dilution.
9. Calculate the volume of cell suspension corresponding to 1.25 x 10^5 cells, plate the appropriate volume of cells in a petri dish, add 10mL of culture medium and incubate. The rest are used for experimental work.

AZ Channel Master

Dummy Layer

1. Dry a clean wafer under nitrogen gas and bake for 10 minutes at 200°C

2. Cool for 5 minutes
3. Set spin coater to following:
i. 10s at 500rpm ACL: 100rpm/s
ii. 60s at 3000rpm ACL: 500rpm/s
iii. 10s at 0 rpm ACL: 300rpm/s
4. Pour SU-8 10 on the wafer ant rotate wafer to allow SU-8 10 fully cover the wafer surface
5. Run spinner
6. Carefully remove wafer from spinner ensuring no drips fall on the wafer surface as the lid opens
i. Ensure the photo resist layer quality is satisfactory. It is a bonding layer so perfection is not necessary as long as the layer is smooth and complete
ii. If the layer quality is not satisfactory put it back in the spinner and clean with acetone and IPA. Dry and go back to 4
7. Pre-bake for 2 minutes at 75 °C, then 5 minutes at 105 °C
i. After 1.5 minutes increase the temperature, set timer for 5.5 minutes
8. Allow baked wafer to cool for 5 minutes
9. Blank exposure for 20 s
10. Post-bake for 1 minute at 75 ° C and 2 minutes at 105 °C
i. After 30s up the temperature, set the timer to 2.5 min to ensure safer is at temperature for at least 1.5 minutes
11. Develop for 2 minutes, IPA (isopropanol) rinse

Channel Layer (Target Height Of Sensing Channel Is 20μm)

12. Set spin coater to the following:
i. 5s at 300 rpm ACL=100
ii. 60s at 1800 rpm ACL=600
iii. 10s at 500 rpm ACL =400
iv. 10s at1000 rpm ACL =250
v. 5s at 0 rpm ACL =200
13. Pour on AZ 4620 and rotate wafer to coat entire surface
14. Run spinner
15. Remove wafer and make sure no drips on surface
i. Ensure the photo resist layer quality is satisfactory. It is a bonding layer so perfection is not necessary as long as the layer is smooth and complete
ii. If the layer quality is not satisfactory put it back in the spinner and clean with acetone and IPA. Dry and go back to 13
16. Bake for 85s at 110 °C
17. Let cool for 5 minutes. Pour on AZ 4620 rotate wafer to coat entire surface
18. Set spinner:
i. 5s at 300 rpm ACL=100
ii. 60s at 1000 rpm ACL=200
iii. 10s at 500 rpm ACL=200
iv. 10s at 1000rpm ACL=250

v. 5s at 0 rpm ACL = 200
19. Run spinner
20. Remove wafer from the spinner and ensure no drips on wafer surface
i. Ensure the photo resist layer quality is satisfactory. It is a bonding layer so perfection is not necessary as long as the layer is smooth and complete
ii. If the layer quality is not satisfactory put it back in the spinner and clean with acetone and IPA. Dry and go back to 17
21. Bake for 165s at 110 °C
22. Let cool for 5 minutes
23. Wait 1 hour to 2 hours (during which SU 8 valve layer can be made) to rehydrate the AZ layer. Tear a white wipe into strips and wet them. Place them around the wafer inside
petri dish and cover. Do not let the strips touch the wafer.
24. Expose for 60s. Time may vary depending on bulb intensity adjustments. Can try 45
s if too long, or vary at your own discretion.
25. Develop for 5 min in AZ developer. Prepare two dishes, pour AZ developer into both.
Place the wafer into the first dish for 1.5min and then move it to the second dish.
Constantly agitate. Quickly empty the first dish and replace the developer. At 3 min put the wafer into the other dish. If you notice that all the exposed AZ has been removed, take it out (No need for full 5 minutes).
26. Rinse with DI water and blow dry (if residue exist, do a quick submersion in developer)
27. Reflow: bake for 5 minutes each at 75 °C and 10 °5C or 75 °C, 105 °C, and 135 °C for greater height drops. Wait until 30s is left in the current time interval and then up the temperature, i.e. increase from 75 °C to 105 °C at 4.5 minutes, or from 105 °C to 135 °C at 9.5 minutes.
28. Check heights and widths with Dektak. If height is much lower, might be the bottle of AZ that is an issue. Order more if results are not consistent, even if the expiration date has not been reached. The photoresist is known to be more difficult to work with than
SU-8.
29. Lastly, higher channel height can be done using three layers of AZ. Can repeat the spin coater conditions for the second layer. Only the speed in step ii) needs to be altered.
The third layer's bake should be for 240s at 110 °C.

SU-8 Valve Master

1. Blow dry cleaned wafer and back for 10 minutes at 200°C to remove water.
2. Let dry for 5 minutes.
3. Set hotplate to 65°C.
4. Set spin coater to following:
i. 10s at 500rpm ACL: 100rpm/s
ii. 60s at 3000rpm ACL: 500rpm/s
iii. 10s at 0 rpm ACL: 300rpm/s
5. Pour SU-2050 on wafer and rotate for a good coverage, then place on it on the spin
coater, center it, and apply vacuum. This will be for ~40μm tall features.
7. Run spin coater.
8. Place wafer on 65°C hot plate and immediately dial up to 95 °C. Set timer for 7 minutes.

Ideally, wafer is at ~65 °C for 30s and 95 °C for at least 6 minutes.
9. Let cool for 5 minutes.
10. Make sure one hotplate is ready at 65 °C again.
11. Expose 12s (adjust as necessary and mind changes to lamp intensity).
12. Take exposed wafer and place on 65 °C hotplate. Set timer for 6.5 minutes. After 30s, dial up to 95 °C. Ideally, wafer is at 65 °C for 1 minute and 95 °C for 5.5 minutes.
13. Let cool for 5 minutes.
14. SU-8 development for 5 minutes, then rinse with IPA at the end and blow dry with N_2 gun.

Device Fabrication

NOTE:
Before using Valve and Channel Masters, treat them with (tridecafluoro-1,1,2,2-tetrahydrooctyl)trichlorosilane. Place a wafer into vacuum chamber and pipette 1µL of the aminosilane onto the weighing boat. Apply vacuum for 5 minutes. Then stop the vacuum but do not open the t-junction valve. Allow wafer to sit inside vacuumed environment for 1 hour before allowing air back in.

Channel Layer

1. Prepare PDMS in a ratio of 1:20, curing agent to base. Aim for ~11 grams of total mass.
2. Mix for 5-6 minutes.
3. Vacuum for ~1 hour.
4. Bring the AZ channel master and the weighing boat with the PDMS into the clean room.
5. Set spin coater to following:
i. 10s at 500rpm ACL: 100rpm/s
ii. 33s at 2000rpm ACL: 500rpm/s
iii. 10s at 0 rpm ACL: 200rpm/s
6. Blow wafer with N_2 gun to get rid of any dust and center the wafer on spin coater
7. Pour the PDMS carefully, so as to not create air bubbles. Do it slowly and try to cover as much of the surface around the center of the wafer as possible.
8. Spin, and then remove the wafer and place it into a petri dish.
9. Streaks will disappear as the PDMS relaxes.
10. Allow the relaxation to occur by using this time to clean up the spin coater.
11. Bring the dish out and bake in oven for 20min at 80C.

Valve Layer

1. Tape the wafer to a circular acrylic frame. Place both into the large petri dish. This will create a well around the wafer for the PDMS to be poured into. Acrylic frame is not necessary if a dish can be found that is around the same diameter as the wafer. Wafer needs to be taped down.

2. Prepare PDMS in a ratio of 1:7, curing agent to base. Depending on the petri dish, the final mass will vary.
3. Mix the PDMS for 5-6 minutes
4. Pour the PDMS into the petri dish and over the valve master
5. Vacuum for ~1 hour
6. Take the dish out, place the lid on it, and bake in over for 24 minutes at 80°C.

PDMS Bonding

1. With both valve and channel wafers baked, take them out and bring into clean room
2. Cut out PDMS blocks from the valve master
3. Each one should be cleaned with scotch tape, on both sides
4. Place a white wipe on the counter and stick a long, looped, piece of scotch tape on it. All PDMS debris should be stuck to this tape to keep the counter clean
5. Punch holes in the valve layer PDMS blocks using the 0.75mm biopsy punches
6. Use scotch tape to clean the biopsy punch between punches to minimize PDMS debris sticking to the punched holes
7. Can blow the punched holes with the N_2 gun as well
8. All PDMS blocks that have been punched should be again cleaned with scotch tape
9. Place a piece of scotch tape on the side of the block that is to be bonded to the channel layer and lay these devices on their back (the side not to be bonded) on a white wipe as you punch additional devices. The counter is generally not clean and the tape will also keep that surface clean as you work.
10. When ready, plasma both the channel wafer and the PDMS block, 30 s at 30 Watts.
11. Align carefully and repeat as necessary. Remember to turn off the lid vacuum before lifting the lid. Use tweezers to carefully remove the dummy block with the glass slide so as to not lift and pull on the valve block
12. When all devices have been bonded to the channel wafer, bring it out inside in a petri dish and bake for at least 1 hour at 80°C . Can be overnight or 24 hours.

Electrode Preparation

1. The glass slides with the electrodes contain more than one set. To cut out individual pieces to make devices, use the diamond scribe and scratch a line where the separation is desired. Do not repeatedly scratch.
2. Place the slide on a counter or table, with the piece to be broken off hanging over the side of the countertop or tabletop.
3. Apply even pressure with your thumb on the section to be broken off and hold the slide firmly. It should fracture nicely at the line that was scratched.
4. Clean these with water and ethanol, then blow dry with the N_2 gun and cover them in a petri dish to be brought into the clean room.

Final Device Assembly

1. After the PDMS baking is done, bring them into the clean room with electrodes
2. Cut around each PDMS block with the scalpel and gently peel them off from the wafer
3. Clean the top and bottom sides with scotch tape
4. Again, prepare white wipes and scotch tape to collect PDMS debris
5. Punch and clean in the same way as the PDMS bonding protocol
6. Blow the glass pieces with the N_2 gun before putting them in the plasma bonder with the PDMS blocks
7. Plasma 30s at 30 Watts
8. The stage for the aligner should be the small circular and not the big square one that is used for wafers
9. Apply a suction vacuum to the stage and place a dummy block on it. The main PDMS block will be placed on top of this one to give it enough height.
10. The piece of glass with the electrodes will need to be taped to a glass slide. Tape it on the left and right sides, avoiding the electrode metal and not in the region that will be covered by the PDMS block.
11. Invert the glass slide with the electrodes on it and place in the vacuum region of the aligner lid
12. Align carefully and remember to turn off the lid vacuum before raising it. Use tweezers to remove the device from the dummy block
13. When finished, place all devices in a petri dish and bake in oven for at least 1 hour at 80°C

Bonding Wires

1. After the assembled device has been baked, cut two pieces of appropriate length wires for each device
2. Do not use the wires that are woven from many smaller threads. Use the one that is a single solid piece
3. Using the wire stripper, remove a section of the rubber sheath from each end, as these sections will be used to make electrical contact
4. Use regular epoxy glue to hold the two wires in place, attaching them to the glass of the device before applying the silver epoxy
5. Use silver epoxy to connect the wires to the pads of the electrodes.
6. After applying the silver epoxy, each device must be baked in the oven for at least 1 hour at 80°C to ensure the silver epoxy cures.
7. Use a voltmeter to check for conductivity and to ensure there are no shorts
8. These wires must be soldered to two points within the aluminum block setup on the microscope stage. After this is done, check that each wire is not shorted with the metal surface surrounding the soldering points using the voltmeter

Lift-off Process

1. Clean using sonicator
2. Setup Wrap a hot plate with aluminum foil. Program the spin coater:
a. 10s at 500 RPM, ACL = 015

b. 30s at 3000 RPM, ACL = 010
c. 20s at 200 RPM, ACL = 005
Set the mask aligner timer to 15s, and position your mask.
3. 10 min at 200ºC Place slides on hot plate at 200°C for 10 minutes, then let cool 2 minutes. This step removes any adsorbed humidity from the surface of the slides.
4. Spin coat Place a slide on the spin coater (slide attachment) and vacuum in place. Use the Pasteur pipette to dispense ~1 mL of S1813 photoresist.
5. Pre-bake 60s at 95ºC Place slide on hot plate for 60s at 95ºC.
6. UV Expose 15s; Place slide on stage. Close lid, make final positioning adjustments and bring the stage up until you feel resistance, and then slide under the lamp.
7. Toluene soak 60s + N_2 dry; Place slide in toluene dish for 1 minute. In this step, the top of the photoresist is being chemically modified to develop slower than resist underneath (top is less oluble). This leads to undercut features favorable to lift-off. Dry with high-purity nitrogen.
8. Post-bake 15s at 95ºC Place slide on hot plate, and bake for 15s. Remove with tweezers, place on aluminum foil for 1 minute cooling.
9. Develop in diluted Tetramethylammonium hydroxide (TMAH) + N_2 dry Create a solution of diluted TMAH: 6 mL of TMAH in 76 mL of deionized water in the glass dish, and place above a (cool) hot plate. The first slide that is immersed will likely be wasted, as the solution is initially aggressive and must be removed at 45 s. As more and more slides are exposed, the solution slowly loses its potency (development time can reach 2 minutes eventually). TMAH solution can be replaced after at least four slides It is very important not to overdevelop (will see cracking of photoresist around features). After development, use the tweezers to transfer a slide to a glass beaker with deionized water. Rinse the slide gently in the water for 1 minute by moving it in and out. N_2 dry. Use a gentle stream as it is possible to blow of features.
10. Microscope verification: Use the microscope to verify slide quality, and adjust procedure as necessary. Place slides into case with photoresist side all facing one way, label the bottom of the case using a piece of tap indicating the direction. Blow the inside of the case with the N_2 gun in the clean room beforehand to clean it. Once outside do not open the case.
11. Metal deposition: Once 20 slides are complete (1 batch), deposit a 50nm Au layer with 5nm Ti or Cr adhesion layer. This can be performed at the Carleton University MicroFabrication Facility. Use e-beam evaporation.
12. Lift-off with N-Methyl-2-pyrrolidone Use NMP to etch the photoresist, leaving only the metal-on-glass electrodes. The etchant should be heated to 70ºC to accelerate the process. Use a magnetic stir bar but be careful not to let your slides get under the stir bar. Use a reasonable spin speed as to not have excessive splashing. The crystallization dish can fit 3 slides at once. This process generally takes 30 minutes. Rinse with deionized water after most of the gold has flaked off. Residual gold can be removed using the squirt bottle's jet. Blow dry gently.

Wet-etching with Aqua Regia and Hydrofluoric Acid

1. Bring all slides into clean room, bake off water at 200°C for 10 minutes, let cool for 2 minutes, and place into case. Mind the top face of the slides. All slides facing up during piranha should remain face up, and this same face should all be aligned in the same direction in the case. Indicate inside the case with tape the side of the slides that is to have metal deposited.

2. Request 50nm Au and 5nm Ti or Cr using electron beam evaporation
3. When slides come back, bring into clean room. Set spin coater to 500 rpm 10s 1000 rpm for 30s, and 10s to ramp down.
4. Use positive photoresist. It should be poured into a smaller bottle and dispensed onto the slide using a glass pipette. Can use S1813 or AZ.
5. Exposure is 60s. Rinse with
water squirt bottle and dip slide in and out of beaker with DI water for 1 minute. Blow dry
6. Bring slides out of clean room. Some photoresist may not be removed. If that is the case, place them under the stereo microscope and scratch off the photoresist with the Exacto knife. The regions you need to scratch off are areas where the covered gold would bridge each pair of electrodes. You must avoid a short.
7. To etch gold, prepare Aqua Regia. The speed and strength is dependent on how much
water is used. E.g. 1:1 acid solution to water. HCl to nitric is 3:1. Recommend 30mL HCL, 10mL nitric, and 40mL water. Also prepare separate water bath.
8. When prepared, use immediately, Notice the gold vanish.
9. Pull it out place it into the water bath. After all slides are done, remove them from the
water bath one by one and rinse with DI water bottle, then blow dry. The underlying Ti or Cr will appear dark/black if compared to a normal glass slide.
10. The etchants for these metals work by removing the metal oxide layer, regenerating it, and repeating. If adhesion layer is Cr, use commercial Cr/CrO etchant. Pour enough to cover a glass slide into a dish and prepare a separate water bath. In our experience, 10-15 s with agitation is enough to remove Cr. After, place slide into water bath, dump etchant into acid waste beaker, and pour in some more for next slide. When finished, rinse slides with DI water again, and blow dry. Check that the adhesion layer is removed with voltmeter by touching down in two blank areas on the slide.
11. If adhesion layer is Ti, buy commercial etchant
12. Prepare one dish with HF and one dish with water. Keep sink water running at all times.
Rinse gloves thoroughly after handling bottle. Ben made a white dipper, you can place two slides onto it, and then place dipper into the HF bath with slides submerged.
13. Rotate and move slides by moving dipper, for about 30 s. Lift dipper up—not out of the dish itself, just above the surface of the HF—and carefully pour out as much solution as possible back into the dish.
14. Dunk dipper into your water bath and bring the whole thing to the sink. Place the dish below the water stream and let it fill to the full volume and overflow for a bit. Then pour out the water and repeat 3-4 times. Make sure the dish, dipper, and your gloves are thoroughly rinsed.
15. Blow dry the slides. Dump the used HF into your waste container, then rinse dish with water three times. Pour in fresh HF and prepare a fresh water bath in the second dish and repeat for more slides.
16. Remove the protective photoresist layer. Use the acetone squirt bottle, and then follow up with isopropanol. Then blow dry. Make sure solvents do not get on the gloves and then are blown onto the slide. Degradation occurs and if you blow in the direction of the electrodes, it will smear on them.
17. Finally, inspect for physical defects under microscope

Appendix II –Setup

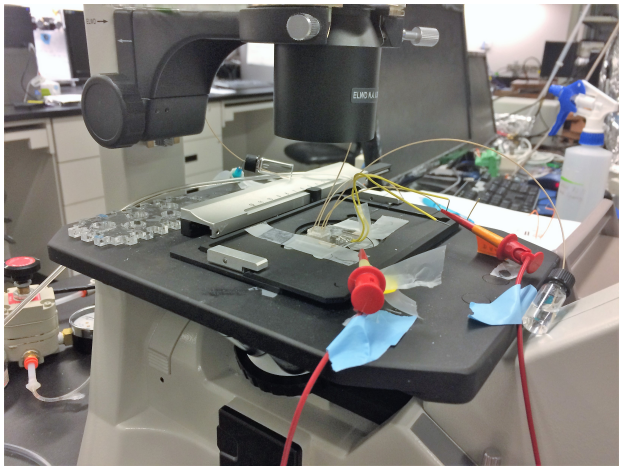

A close-up image of the transfection and impedance measurement device and its corresponding electronic and pressure connections on a microscope

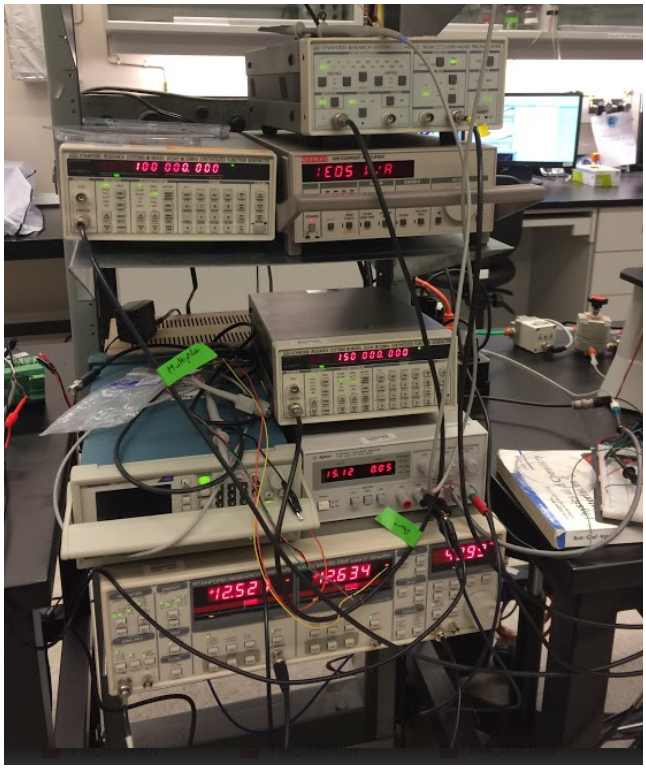

A photograph of the electronic setup as described in detail in section 2.2

Appendix III –channel designs

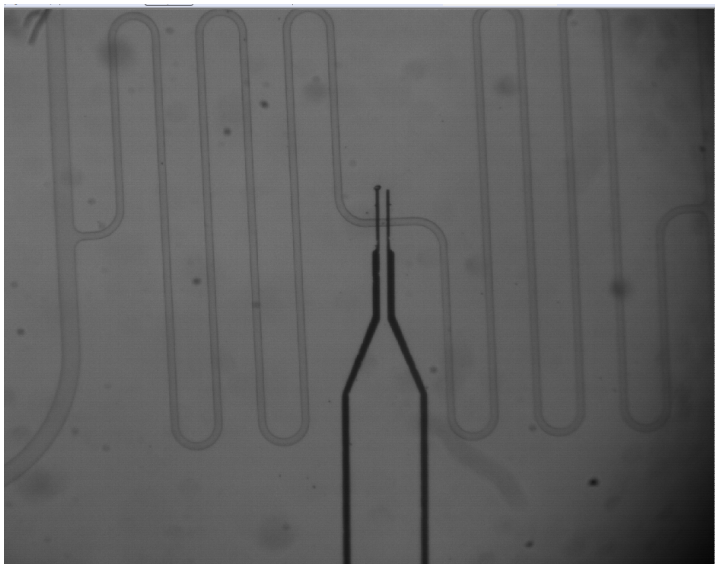

A microscope image of electrodes under an H-channel design, where the central channel is made in the form of a serpentine for improved flow control and reduced flow rate; used for preliminary impedance tests